Available online at www.pelagiaresearchlibrary.com

Pelagia Research Library

Pelagia Research Library

Advances in Applied Science Research, 2016, 7(4):127-149

Pelagia Research Library

ISSN: 0976-8610
CODEN (USA): AASRFC

Soret and Dufour Effects on Double-Diffusive Heat Transfer Flow in a Rectangular Duct with Radiation Absorption and Non-linear Density-Temperature Relation

G. Sreedevi[1*], D. R. V. Prasada Rao[2] and G. Venkata Ramana Reddy[1]

[1]*Department of Mathematics, K. L. University, Green Fields, Vaddeswaram, Guntur 522502, A.P, India*
[2]*Department of Mathematics, S. K. University, Anantapur-515003, A.P, India*

ABSTRACT

We analyze the effect of magnetic field on convective heat and mass transfer flow of a viscous electrically-conducting fluid through a porous medium in a rectangular duct with Soret, Dufour, chemical reaction, and thermal radiation effects. The equations governing the flow, heat and mass transfer are solved by employing the Galerkin Finite element analysis with tri-nodal triangular elements. The temperature and concentration distributions are analyzed for different values of M, Q, Rad, S_0, Du and γ. The rates of heat and mass transfer are evaluated numerically for different parametric values. The numerical results obtained in the present paper are validated by favorable comparison with previous published results.

Keywords: Heat and Mass transfer; Rectangular duct; Hartmann number; Soret and Dufour effect; Thermal radiation; Radiation absorption; Non-linear density-temperature relation.

Nomenclature

a, b, c non-dimensional variable
C concentration
Cc concentration on cold wall
Ch concentration on warm wall
Cp specific heat at constant pressure
D^{-1} inverse Darcy parameter
Du, Daf Dufour parameter
G Grashof number
g′ acceleration due to gravity
H_0, $\overline{H}$ strength of the magnetic field
k permeability of the porous medium
K chemical reaction parameter
kf thermal conductivity
K_{11} cross diffusivity
M Hartmann number
N buoyancy ratio
N_1(Rad) thermal radiation parameter
Nu Nusselt number
Pr Prandtl number
p′ pressure
Q radiation absorption
qr radiative heat flux
Ra Rayleigh number
So Soret parameter
Sc Schmidt number
Sh Sherwood number
T′ temperature
Tc temperature at the cold wall
Th temperature at the warm wall
u, v velocity components
u′, v′ Darcy velocities
x horizontal coordinate
y vertical coordinate

Greek symbols

α heat source parameter
β_0,β_1 thermal expansion coefficients
β^* volume coefficient of expansion with mass fraction concentration
φ dimensionless heat generation or absorption
μ coefficient of viscosity
μ_e magnetic permeability
ν kinematic viscosity
θ dimensionless temperature
ρ density of fluid
σ electrical conductivity
Ω verticity
Ψ dimensionless stream function
ϕ stream function
γ non–linear density temperature relation
Γ *condensate mass flow rate*

Subscripts

c cold wall
h warm side wall

INTRODUCTION

Advanced studies in the convective heat and mass transfer in porous medium provided greater industrial standing and generated research interest in many academicians and scientists. Equally, natural convection, the genesis of

which is due to the effect of density difference in a body force fluid resulted from a difference in temperature or concentration parameters, plays a key role in wider industrial applications. Natural convection adversely affects local growth conditions and enhances the overall transport rate. The combination of temperature and concentration gradients in the fluid will lead to buoyancy-driven flows. This has an important influence on the solidification process in a binary system. When heat and mass transfer occurs simultaneously, it leads to a complex fluid motion called double-diffusive convection.

Studies related to double-diffusive MHD boundary layer flow with heat and mass transfer over flat surfaces are extremely important and have many applications in engineering and industrial processes. For instance, heat and mass transfer occur in processes, such as drying, evaporation at the surface of a water body, and energy transfer in a wet cooling tower, cooling of nuclear reactors, MHD power generators, MHD pump, chemical vapor deposition on surfaces, formation and dispersion of fog, and distribution of temperature and moisture over agriculture fields. Double-diffusion occurs in a wide range of scientific fields such as oceanography, astrophysics, geology, biology and chemical processes. Extensive study was made by Ostrach *et al.* [1] and Viskanta *et al.* [2] on this given subject. A fundamental study of scale analysis relative to heat and mass transfer within cavities submitted to horizontal combined and pure temperature and concentration gradients was analysed by Bejan [3]. An experimental study has been done by Kamotani *et al.* [4] considering natural convection in shallow enclosures with horizontal temperature and concentration gradients. Similar experimental studies on thermo-solutal convection in rectangular enclosures were reported by Lee and Hyun [5] and Lee *et al.* [6] in unsteady double-diffusive convection in a rectangular enclosure with aiding and opposing temperature and concentration gradients. Ranganathan and Viskanta [7], Trevisan and Bejan [8], Beghein *et al.* [9] and Nishimura *et al.* [10] and others extended the related numerical studies dealing with double-diffusive natural convection in cavities. Sivaiah [11] investigated double-diffusive convective heat transfer flow of a viscous fluid through a porous medium with rectangular duct with thermo-diffusion by using the finite-element technique. Chamkha and Al-Naser [12] have investigated the hydromagnetic double-diffusive convection in a rectangular enclosure with opposing temperature and concentration gradients. Shanthi *et al.* [13] have investigated double-diffusive flow in a rectangular cavity using Darcy model. They have analyzed the effect of dissipation radiation on the double-diffusive flow of a viscous fluid in the rectangular cavity. Farhany and Tarun [14] numerically studied the double-diffusive natural convective heat and mass transfer in an inclined rectangular cavity filled with porous medium.

Several applications were witnessed in the industry of fluids that are electrically conducting induced by magnetic field. Oreper and Szekely [15] studied the effect of an externally imposed magnetic field on buoyancy driven flow in a rectangular cavity and found that the presence of a magnetic field can suppress natural convection currents. Magnetic and gravitational natural convection of melted silicon-two dimensional numerical computations for the rate of heat transfer was studied by Ozoe and Maruo [16]. Natural convection heat transfer in rectangular enclosures with traverse magnetic field were studied by Garandet *et al.* [17] and Alchaar *et al.* [18]. The effects of magnetic field on free convection in a rectangular enclosure was studied by Rudraiah *et al.* [19]. Numerical study of laminar natural convection in tilted enclosure with transverse magnetic field was investigated by Al-Najem *et al.* [20]. Yu et al. [21] numerically investigated the natural convection in a rectangular cavity under different directions of uniform magnetic field.

The study of natural convection heat transfer induced by internal heat generation has assumed much importance over time due to several applications in geophysics and energy-related engineering problems. Such applications include heat removal from nuclear fuel debris, underground disposal of radioactive waste materials, storage of foodstuff, and exothermic chemical reactions in packed-bed reactor. In a numerical study of two-dimensional natural convection of air in an externally heated vertical or inclined square box containing uniformly distributed internal energy sources conducted by Acharya and Goldstein [22], it was found that the average heat flux ratio along the cold wall increased with increasing external Rayleigh numbers and decreasing internal Rayleigh numbers. Their studies also revealed two distinct flow pattern systems depending on the ratio of the internal to the external Raleigh numbers. Churbanov *et al.* [23] investigated unsteady natural convection of a heat generating fluid in a vertical rectangular enclosure with isothermal or adiabatic rigid walls. Similar related works dealing with temperature-dependent heat generation effects were studied by Vajravelu and Nayfeh [24] and Chamkha [25]. A numerical investigation of the steady MHD free convection in a rectangular cavity filled with a fluid-saturated porous medium and with internal heat generation was studied by Grosan et at. [26]. Reddy and Narasimhan [27] investigated heat generation effects in natural convection inside a porous annulus. The effect of magnetic field on mixed convection heat transfer in a lid-driven square cavity was studied by Baker et al. [28].

Viscous dissipation, a partially irreversible process, which happens due to shear forces transforming heat into fluid flow, has been studied by many researchers for different geometries. Verschoor *et al.* [29] have studied the effect of viscous dissipation and radiation on unsteady MHD free convection flow fast vertical plate in porous medium. They

found that the temperature profile increases when viscous dissipation increases. Barletta and Pulvirenti [30] studied the forced convection with slug flow and viscous dissipation in a rectangular duct. Van Rij et al. [31] investigated the effect of viscous dissipation and rarefaction on rectangular micro channel convective heat transfer. Padmavathi [32] Nagaradhika [33] and Sreenivasa [34] have analyzed the connective heat transfer through a porous medium in a rectangular cavity with heat sources and dissipation under varied conditions. Umavathi and Odelu [35] studied the effect of variable viscosity on free convection in a vertical rectangular duct. Umavathi and Sheremet [36] further studied the viscous dissipation and the influence of temperature dependent conductivity of a nanofluid in a vertical rectangular duct.

Thermal radiation plays a significant role in many engineering applications particularly when the temperature is high. In the case of free convection or when the effects of variable properties are also included, the energy transformation can be a function of difference between T_1 and T_0. Radiation contributes significantly to the transfer of energy in furnaces, chambers of combustion, rocket plumes, heat exchangers under high temperatures, nuclear reactors and the like. On the other hand, in case of conduction and convection are suppressed, thermal radiation plays an important role during heat transfers even at temperatures of lower degrees like in thermos bottles and space craft thermal control. Makinde [37] studied free convection flow with thermal radiation and mass transfer past a moving vertical plate. Chiu *et al.* [38] studied the mixed convection heat transfer in horizontal rectangular ducts with radiation effects. Sakurai et al. [39] studied the radiation effects on mixed turbulent natural and forced convection in a horizontal channel using direct numerical simulation and found that the radiation effect changes the distributions of the temperature fluctuation intensity and the turbulent heat flux. Mahapatra et al. [40] studied the mixed convection flow in an inclined enclosure under magnetic field with thermal radiation and heat generation. Recently, Lee et al. [41] investigated the characteristics of premature and stable critical heat flux for downward flow boiling at low pressure in a narrow rectangular channel. Liu et al. [42] reviewed the near-field thermal radiation and brought out the recent applications in the subject. Sheikholeslami et al. [43] numerically studied the MHD free convection of Al_2O_3-water nanofluid considering thermal radiation.

Heat transfer occurs through insulation materials by conduction, while heat loss to or gaining of heat from atmosphere occur by means of convection and radiation. Materials, which have low thermal conductivity, are those, which have a high proportion of small voids containing air. These voids are not big enough to transmit heat by convection or radiation and therefore the rate of heat transfer reduces. The mass flux created by a temperature gradient and the energy flux resulted by concentration differences is known as thermal-diffusion (Soret) effect and diffusion-thermo (Dufour) effect respectively. The importance of the Soret and Dufour effects are visible in many practical applications preferably in areas such as geosciences chemical engineering etc., Cheng [44] investigated the Soret and Dufour effects on natural convection boundary layer flow over a vertical cone in a porous medium with constant wall heat and mass fluxes. Chamkha *et al.* [45] studied the hydromagnetic double-diffusive convection in a rectangular enclosure with linearly heated and concentrated wall(s) in the presence of heat generation/absorption effects. Motozawa *et al.* [46] experimentally investigated on the heat transfer characteristics in rectangular duct flow of a magnetic fluid under magnetic field. Umavathi and Chamkha [47] studied natural convection flow in a vertical rectangular duct with isothermal wall boundary conditions. Chamkha *et al.* [48] studied heat and mass transfer in a porous medium filled rectangular duct with Soret and Dufour effects under inclined magnetic field. Zhang and Huang [49] studied the effect of magnetic obstacle on fluid flow and heat transfer in a rectangular duct. Stelian [50] studied the MHD effects in turbulent duct flows under the influence of transverse uniform and non-uniform magnetic fields. Recently, Srinivasacharya and Himabindu [51] studied effect of magnetic field on entropy generation due to micropolar fluid flow in a rectangular duct. Kishan and Sekhar [52] applied the Finite element analysis to study the fully developed unsteady MHD convection flow in a vertical rectangular duct with viscous dissipation and heat source/sink. Wang [53] brought out analytic solutions for pulsatile flow through annular, rectangular and sector ducts filled with a Darcy–Brinkman medium.

In this paper, we investigate the effect of magnetic field on convective heat and mass transfer flow of a viscous electrically-conducting fluid through a porous medium in a rectangular cavity with thermal radiation and dissipative effects. To determine the surface porosity, a closely packed porous material with respect to the structure of the pore space of the porous medium is considered. The duct is filled with saturated porous medium, and the flow of the working fluid was analyzed using a Darcy model which takes into account buoyancy and all the remaining effects of the rectangular duct. The equations governing the flow, heat and mass transfer are solved by employing the Galerkin Finite element analysis with tri-nodal triangular elements. The temperature and concentration distributions are analyzed for different values of M, Q, Rad, So, Du and γ. The rates of heat and mass transfer are evaluated numerically for different parametric values.

1. Problem Formulation

We consider the mixed convective heat and mass transfer flow of a viscous incompressible fluid in a saturated porous medium confined in the rectangular duct as shown in Fig. 1 whose base length is *a* and height *b*. The heat flux on the base and top walls is maintained constant. The Cartesian coordinate system O (x,y) is chosen with origin on the central axis of the duct and its base parallel to x-axis.

We assume that

(a) The convective fluid and the porous medium are everywhere in local thermal equilibrium with the solid matrix .
(b) There is no phase change of the fluid in the medium.
(c) The properties of the fluid and of the porous medium are homogeneous and isotropic (uniform with a constant porosity and permeability)
(d) The porous medium is assumed to be closely packed so that Darcy's momentum law is adequate in the porous medium.
(e) The effect of buoyancy force is acting on the fluid. So, well known Boussinesq approximation is applicable.
(f) The magnetic Reynolds number is assumed to be small so that the induced magnetic field can be neglected compared to the applied magnetic field.

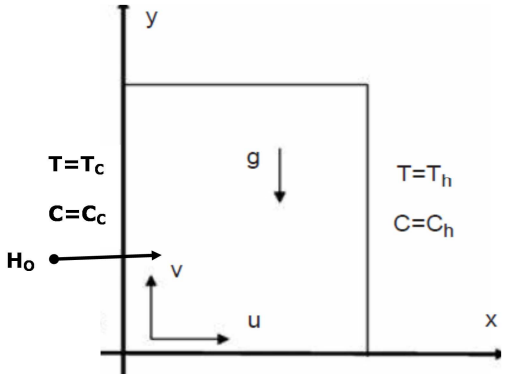

Fig. 1 Schematic Diagram of the Problem

In this problem we follow Darcy model (as fluid flow is through a porous medium), in momentum equation and considering Boussinesq approximation with magnetic field $\overline{H}$. Under these assumption the momentum equations in the x and y directions are as follows (Revnic et al. [54])

$$0 = -(\frac{\mu}{k})u' - \frac{\partial p}{\partial x'} - \frac{\sigma\mu_e^2 H_o^2}{\rho'}$$

$$0 = -(\frac{\mu}{k})v' - \frac{\partial p}{\partial y'} - \frac{\sigma\mu_e^2 H_o^2}{\rho'}(v_1') - \rho'\overline{g}$$

Eliminating the pressure p by cross differentiation of above two equations, we get

$$0 = -(\frac{\mu}{k})(\frac{\partial u'}{\partial y'} - \frac{\partial v'}{\partial x'}) + \frac{\sigma\mu_e^2 H_o^2}{\rho'}(-\frac{\partial u'^2}{\partial y'} + 2\frac{\partial v'}{\partial y'} + \frac{\partial v'^2}{\partial x'}) + \frac{\partial}{\partial x'}(\rho'\overline{g})$$

Under these assumptions, the governing equations of the present work are based on the balanced laws of mass, momentum energy and concentration in two dimensions. Following the assumptions of the magnetic field used by Chamkha and Al-Naser [12], the governing equations can be written in the form of dimensional equations as

$$\frac{\partial u'}{\partial x'} + \frac{\partial v'}{\partial y'} = 0 \quad (1)$$

$$u' = -\frac{k}{\mu}\left(\frac{\partial p'}{\partial x'}\right) \quad (2)$$

$$v' = -\frac{k}{\mu}\left(\frac{\partial p'}{\partial y'} + \rho' g\right) - (\frac{\sigma\mu_e^2 H_o^2}{(\mu/\rho)})v \quad (3)$$

$$\rho\sigma^c p\left(u'\frac{\partial T'}{\partial x'} + v'\frac{\partial T'}{\partial y'}\right) = k_f\left(\frac{\partial^2 T'}{\partial x'^2} + \frac{\partial^2 T'}{\partial y'^2}\right) + Q(T_0 - T) - \frac{\partial(q_r)}{\partial x} + \frac{D_m K_T}{C_s C_p}\left(\frac{\partial^2 C}{\partial x'^2} + \frac{\partial^2 C}{\partial y'^2}\right) \quad (4)$$

$$\left(u'\frac{\partial C}{\partial x'}+v'\frac{\partial C}{\partial y'}\right)=D_1\left(\frac{\partial^2 C}{\partial x'^2}+\frac{\partial^2 C}{\partial y'^2}\right)+\frac{D_m K_T}{K_m}\left(\frac{\partial^2 T}{\partial x'^2}+\frac{\partial^2 T}{\partial y'^2}\right)-k'C \tag{5}$$

$$\rho' = \rho_0\left\{\begin{matrix}1-\beta_0(T'-T_0)-\beta_1(T'-T_0)^2\\ -\beta^{\bullet}(C'-C_0)\end{matrix}\right\}$$

$$T_0=\frac{T_h+T_c}{2}, C_0=\frac{C_h+C_c}{2} \tag{6}$$

where u′ and v′ are Darcy velocities along θ - (x, y) direction. T′, C, p′ and g′ are the temperature, concentration, pressure and acceleration due to gravity, T_c, Cc and T_h, C_h are the temperature and concentration on the cold and warm side walls, respectively. ρ′, μ, ν, β_0 and β_1, are the density, coefficients of viscosity, kinematic viscosity and thermal expansions of the fluid, k is the permeability of the porous medium, k_f is the thermal conductivity, C_p is the specific heat at constant pressure, Q is the strength of the heat source, k_{11} is the cross diffusivity, β* is the volume coefficient of expansion with mass fraction concentration and q_r is the radiative heat flux. σ is the electrical conductivity, μ_e is the magnetic permeability of the medium and H_0 is the strength of the magnetic field. This means that solutions to the ideal MHD equations are only applicable for a limited time for a region of a given size before diffusion becomes too important to ignore.

The boundary conditions for the problem are

u′ = v′ = 0 on the boundary of the duct;
T′ = T_c, C=C_c on the side wall to the left;
T′ = T_h, C=C_h on the side wall to the right; (7)

$\frac{\partial T'}{\partial y}=0$, $\frac{\partial C'}{\partial y}=0$ on the top y = 0 and

Bottom $u=v=0$ walls y = 0 which are insulated.

Invoking the Rosseland approximation for radiation

$$q_r=\frac{4\sigma^*}{3\beta_R}\frac{\partial T'^4}{\partial y}$$

Expanding T^4 in Taylor's series about T_e and neglecting higher-order terms $T'^4 \cong 4T_e^3T-3T_e^4$

We now introduce the following non-dimensional variables

x′ = ax; y′ = by; c = b/a
u′ = (ν/a) u; v′ = (ν/a)v; p′ =($\nu^2\rho/a^2$)pr
T′ = T_0 + θ (T_h – T_c) C′ = C_0 + ϕ (T_h – T_c) (8)

The governing equations in the non-dimensional form are

$$u=-\left(\frac{K}{a^2}\right)\frac{\partial p}{\partial x} \tag{9}$$

$$v=-\frac{k}{a^2}\frac{\partial p}{\partial y}-\frac{kag}{\nu^2}+\frac{kag(\beta_0(T_h-T_c)\theta+\beta_1(T_h-T_c)^2\theta^2)}{\nu^2}+\frac{kag\beta^{\bullet}(C_h-C_c)\phi}{\nu^2}-(\frac{\sigma\mu_e^2H_o^2}{(\mu/\rho)})v \tag{10}$$

$$P_r\left(u\frac{\partial\theta}{\partial x}+v\frac{\partial\theta}{\partial y}\right)=\left(1+\frac{4N_1}{3}\right)\left(\frac{\partial^2\theta}{\partial x^2}+\frac{\partial^2\theta}{\partial y^2}\right)-\alpha\theta+Du\left(\frac{\partial^2\phi}{\partial x^2}+\frac{\partial^2\phi}{\partial y^2}\right) \tag{11}$$

$$Sc\left(u\frac{\partial\phi}{\partial x}+v\frac{\partial\phi}{\partial y}\right)=\left(\frac{\partial^2\phi}{\partial x^2}+\frac{\partial^2\phi}{\partial y^2}\right)-k\phi+ScSo\left(\frac{\partial^2\theta}{\partial x^2}+\frac{\partial^2\theta}{\partial y^2}\right) \tag{12}$$

In view of the equation of continuity, we introduce the stream function ψ as

$$u = \frac{\partial \psi}{\partial y} \quad ; \qquad v = -\frac{\partial \psi}{\partial x} \tag{13}$$

Eliminating p from the Eqs. (9) and (10) and making use of Eq. (11) the equations in terms of ψ and θ are

$$((1+M^2)\frac{\partial^2 \psi}{\partial x^2} + \frac{\partial^2 \psi}{\partial y^2}) = -Ra(\frac{\partial \theta}{\partial x}(1+2\gamma\theta) + N\frac{\partial \phi}{\partial x}) \tag{14}$$

$$P_r\left(\frac{\partial \psi}{\partial y}\frac{\partial \theta}{\partial x} - \frac{\partial \psi}{\partial x}\frac{\partial \theta}{\partial y}\right) = \left(1+\frac{4}{3N_1}\right)\left(\frac{\partial^2 \theta}{\partial x^2} + \frac{\partial^2 \theta}{\partial y^2}\right) - \alpha\theta + Du\left(\frac{\partial^2 \phi}{\partial x^2} + \frac{\partial^2 \phi}{\partial y^2}\right) \tag{15}$$

$$Sc\left(\frac{\partial \psi}{\partial y}\frac{\partial \phi}{\partial x} - \frac{\partial \psi}{\partial x}\frac{\partial \phi}{\partial y}\right) = \left(\frac{\partial^2 \phi}{\partial x^2} + \frac{\partial^2 \phi}{\partial y^2}\right) - k\,\phi + ScSo\left(\frac{\partial^2 \theta}{\partial x^2} + \frac{\partial^2 \theta}{\partial y^2}\right) \tag{16}$$

where

$$G = \frac{g\beta(T_h - T_c)a^3}{\nu^2},\ D^{-1} = \frac{K}{a^2},\ Pr = \mu\, c_p / k_f,\quad \alpha = Qa^2/k_f,\ Ra = G * D^{-1} = \frac{\beta g(T_h - T_c)Ka}{\nu^2},\ N_1 = \frac{3\beta_R K_1}{4\sigma^{\bullet} T_e^3},$$

$$Sc = \frac{\nu}{D_1} \qquad k = \frac{k'a^2}{D_1},\quad So = \frac{D_m K_T (T_h - T_c)}{\nu K_m (C_h - C_c)},\ Du = \frac{D_m K_t (C_h - C_c)}{C_s C_p (T_h - T_c)},\ N = \frac{\beta^* (C_h - C_c)}{\beta(T_h - T_c)},\ M^2 = \frac{\sigma\mu_e^2 H_o^2 a^2}{\nu}$$

are the Grashof number, Porosity parameter, Prandtl number (Pr=0.71), heat source parameter, Rayleigh number, radiation parameter, Schmidt number, chemical reaction parameter, Soret parameter, Dufour parameter, buoyancy ratio, and the Hartmann number, respectively.

The four dimensionless boundary conditions are

$$\frac{\partial \psi}{\partial x} = 0, \frac{\partial \psi}{\partial y} = 0 \ on \ \ x = 0\ ,\ \ \theta = 1,\ \phi = 1 \quad \text{and} \tag{17}$$

$$\frac{\partial \psi}{\partial x} = 0, \frac{\partial \psi}{\partial y} = 0 \ on \ \ x = 1\ ,\ \theta = 0, \phi = 0 \tag{18}$$

2. Finite-Element Analysis and Problem Solution

The region is divided into a finite number of tri-nodal triangular elements, in each of which the element equation is derived using the Galerkin weighted residual method. In each element f_i, the approximate solution for an unknown f in the variational formulation is expressed as a linear combination of shape function $\left(N_k^i\right)k = 1,2,3,$ which are linear polynomials in x and y. This approximate solution of the unknown f coincides with actual values at each node of the element. The variational formulation results in a 3 x 3 matrix equation (stiffness matrix) for the unknown local nodal values of the given element. These stiffness matrices are assembled in terms of global nodal values using inter-element continuity and boundary conditions resulting in a global matrix equation.

In each case, there are r distinct global nodes in the finite-element domain and f_p (p = 1,2,……r) is the global nodal values of any unknown f defined over the domain then

$$f = \sum_{i=1}^{8} \sum_{p=1}^{r} f_p\ \Phi_p^i$$

where the first summation denotes summation over s elements and the second one represents summation over the independent global nodes and $\Phi_p^i = N_N^i$, if p is one of the local nodes say k of the element $e_i = 0$, otherwise f_p's are determined from the global matrix equation. Based on these lines, we now make a finite-element analysis of the given problem governed by Eqs. (14) through (16) subjected to the conditions Eqs. (17) and (18).

Let ψ^i, θ^i and ϕ^i be the approximate values of ψ, θ and ϕ in an element θ_i

$$\psi^i = N_1^i\ \psi_1^i + N_2^i\ \psi_2^i + N_3^i\ \psi_3^i \tag{19}$$

$$\theta^i = N_1^i\ \theta_1^i + N_2^i\ \theta_2^i + N_3^i\ \theta_3^i \tag{20}$$

$$\phi = N_1^i \phi_1^i + N_2^i\ \phi_2^i + N_3^i\ \phi_3^i \tag{21}$$

Substituting the approximate value ψ^i, θ^i and ϕ^i for ψ, θ and ϕ respectively in Eq. (13), the error

$$E_1^i = \left(1+\frac{4}{3N_1}\right)\frac{\partial^2\theta^i}{\partial x^2}+\frac{\partial^2\theta^i}{\partial y^2}-\Pr\left(\frac{\partial\psi^i}{\partial y}\frac{\partial\theta^i}{\partial x}-\frac{\partial\psi^i}{\partial x}\frac{\partial\theta^i}{\partial y}\right)-\alpha\theta+Du\left(\frac{\partial^2\phi^i}{\partial x^2}+\frac{\partial^2\phi^i}{\partial y^2}\right) \tag{22}$$

$$E_2^i = \frac{\partial^2\phi^i}{\partial x^2}+\frac{\partial^2\phi^i}{\partial y^2}-Sc\left(\frac{\partial\psi^i}{\partial y}\frac{\partial\phi^i}{\partial x}-\frac{\partial\psi^i}{\partial x}\frac{\partial\phi^i}{\partial y}\right)-k\phi^i+ScSo\left(\frac{\partial^2\phi^i}{\partial x^2}+\frac{\partial^2\phi^i}{\partial y^2}\right) \tag{23}$$

Under the Galerkin method, this error is made orthogonal over the domain of e_i to the respective shape functions (weight functions) where

$$\int_{ei} E_1^i\ N_k^i\ d\Omega = 0\,, \qquad \int_{ei} E_2^i N_k^i d\Omega = 0$$

$$\int_{ei=} N_k^i\left(1+\frac{4}{3N_1}\right)\left(\frac{\partial^z\theta^i}{\partial x^2}+\frac{\partial^z\theta^i}{\partial y^2}\right)-\Pr\left(\frac{\partial\psi^i}{\partial y}\frac{\partial\theta^i}{\partial x}-\frac{\partial\psi^i}{\partial x}\frac{\partial\theta^i}{\partial y}\right)$$
$$-\alpha\theta+Du\left(\frac{\partial^z\phi^i}{\partial x^2}+\frac{\partial^z\phi^i}{\partial y^2}\right)d\Omega=0 \tag{24}$$

$$\int_{ei=} N_k^i\left(\frac{\partial^z\phi^i}{\partial x^2}+\frac{\partial^z\phi^i}{\partial y^2}\right)-Sc\left(\frac{\partial\psi^i}{\partial y}\frac{\partial\phi^i}{\partial x}-\frac{\partial\psi^i}{\partial x}\frac{\partial\phi^i}{\partial y}\right)-k\phi^i$$
$$+ScSo\left(\frac{\partial^z\theta^i}{\partial x^2}+\frac{\partial^z\theta^i}{\partial y^2}\right)d\Omega=0 \tag{25}$$

Using Green's theorem, we reduce the surface integral of Eqs. (24) and (25) without affecting the ψ terms and obtain

$$\int_{ei} N_k^i\left\{\left(1+\frac{4}{3N_1}\right)\frac{\partial N_k^i}{\partial x}\frac{\partial\theta^i}{\partial x}+\frac{\partial N_k^i}{\partial y}\frac{\partial\theta^i}{\partial y}-\Pr N_k\left(\frac{\partial\psi^i}{\partial y}\frac{\partial\theta^i}{\partial x}-\frac{\partial\psi^i}{\partial x}\frac{\partial\theta^i}{\partial y}\right)\right.$$
$$\left.-\alpha\theta+Du\left(\frac{\partial N_k^i}{\partial x}\frac{\partial\phi^i}{\partial x}+\frac{\partial N_k^i}{\partial y}\frac{\partial\phi^i}{\partial y}\right)\right\}d\Omega$$
$$=\int_{\Gamma i} N_k^i\left(\left(\frac{\partial\theta^i}{\partial x}+Du\frac{\partial\phi^i}{\partial x}\right)n_x+\left(\frac{\partial\theta^i}{\partial y}+Du\frac{\partial\phi^i}{\partial y}\right)n_y\right)d\Gamma_i \tag{26}$$

$$\int_{eiei} N_k^i\left\{\frac{\partial N_k^i}{\partial x}\frac{\partial\phi^i}{\partial x}+\frac{\partial N_k^i}{\partial y}\frac{\partial\phi^i}{\partial y}-Sc^i N_k\left(\frac{\partial\psi^i}{\partial y}\frac{\partial\phi^i}{\partial x}-\frac{\partial\psi^i}{\partial x}\frac{\partial\phi^i}{\partial y}\right)-k\phi^i+ScSo\left(\frac{\partial N_k^i}{\partial x}\frac{\partial\theta^i}{\partial x}+\frac{\partial N_k^i}{\partial y}\frac{\partial\theta^i}{\partial y}\right)\right\}d\Omega$$
$$=\int_{\Gamma i} N_k^i\left(\left(\frac{\partial\theta^i}{\partial x}+ScSo\frac{\partial\phi^i}{\partial x}\right)n_x+\left(\frac{\partial\theta^i}{\partial y}+ScSo\frac{\partial\phi^i}{\partial y}n_y\right)\right)d\Gamma_i \tag{27}$$

where Γ_I is the boundary of e_i.

Substituting L.H.S. of Eqs. (19) through (21) for ψ^i, θ^i and ϕ^i in Eqs. (26) and (27) we get

$$\sum_1\int_{ei}\left(1+\frac{4N}{3}\right)\frac{\partial N_k^i}{\partial x}\frac{\partial N_L^i}{\partial x}+\frac{\partial N_L^i}{\partial y}\frac{\partial N_k^i}{\partial y}-\Pr\sum_1\psi_m^i\int_{ei}\left(\frac{\partial N_m^i}{\partial y}\frac{\partial N_L^i}{\partial x}-\frac{\partial N_m^i}{\partial x}\frac{\partial N_L^i}{\partial y}\right)d\Omega$$
$$-\alpha\sum\theta^i\int_{ei} N\,N_k\,l\,d\Omega_i+Du\sum_1^3\int_{ei}\left(\frac{\partial N_k^i}{\partial x}\frac{\partial N_L^i}{\partial x}+\frac{\partial N_L^i}{\partial y}\frac{\partial N_k^i}{\partial y}\right)d\Omega$$

$$= \int_{\Gamma_i} N_k^i \left(\left(\frac{\partial \theta^i}{\partial x} + \mathrm{Du}\frac{\partial \phi^i}{\partial x}\right) n_x + \left(\frac{\partial \theta^i}{\partial y} + Du\frac{\partial \phi^i}{\partial y}\right) n_y \right) d\Gamma_i = Q_k^i \, (l, m, k = 1,2,3) \tag{28}$$

$$\sum_1 \int_{ei} \phi^i \left(\frac{\partial N_k^i}{\partial x}\frac{\partial N_L^i}{\partial x} + \frac{\partial N_L^i}{\partial y}\frac{\partial N_k^i}{\partial y}\right) - Sc \sum_1 \psi_m^i \int_{ei} \left(\frac{\partial N_m^i}{\partial y}\frac{\partial N_L^i}{\partial x} - \frac{\partial N_m^i}{\partial x}\frac{\partial N_L^i}{\partial y} \right) d\Omega$$

$$+ ScSo \sum \theta^i \int_{ei} \left(\frac{\partial N_k^i}{\partial x}\frac{\partial N_L^i}{\partial x} + \frac{\partial N_L^i}{\partial y}\frac{\partial N_k^i}{\partial y}\right) d\Omega_i - k \sum_1^3 \phi^i N_k^i N_L^i d\Omega =$$

$$\int_{\Gamma i} N_k^i \left(\frac{\partial \theta^i}{\partial x} + ScSo\frac{\partial \phi^i}{\partial x} \right) n_x + \left(\frac{\partial \theta^i}{\partial y} + ScSo\frac{\partial \phi^i}{\partial y} n_y \right) d\Gamma_i = Q_i^C \, (l, m, k = 1,2,3) \tag{29}$$

where $Q_k^i = Q_{k1}^i + Q_{k2}^i + Q_{k3}^i$, Q_k^i 's being the values of Q_k^i on the sides s = (1,2,3) of the element e_i. The sign of Q_k^i 's depends on the direction of the outward normal with respect to the element.

Choosing different N_k^i 's as weight functions and following the same procedure, we obtain the matrix equations for three unknowns (Q_p^i) viz.,

$$(a_p^i)(\theta_p^i) = (Q_k^i) \tag{30}$$

where (a_{pk}^i) is a 3 x 3 matrix, $(\theta_p^i), (Q_k^i)$ are column matrices.

Repeating the above process with each of s elements, we obtain sets of such matrix equations. Introducing the global coordinates and global values for θ_p^i and making use of inter-element continuity and boundary conditions relevant to the problem, the above stiffness matrices are assembled to obtain a global matrix equation. This global matrix is r x r square matrix if there are r distinct global nodes in the domain of flow considered. Similarly, substituting ψ^i, θ^i and ϕ^i in Eq. (12) and defining the error

$$E_3^i = (1 + M^2)\frac{\partial^2 \psi}{\partial x^2} + \frac{\partial^2 \psi}{\partial y^2} - \mathrm{Ra}\left(\frac{\partial \theta}{\partial x}(1 + 2\gamma\theta) + N\frac{\partial \phi}{\partial x}\right) \tag{31}$$

and following the Galerkin method, we obtain

$$\int_{\Omega} E_3^i \psi_j^i d\Omega = 0 \tag{32}$$

Using Green's theorem, Eq. (28) reduces to

$$\int_{\Omega} \left((1 + M^2)\frac{\partial N_k^i}{\partial x}\frac{\partial \psi^i}{\partial x} + \frac{\partial N_k^i}{\partial y}\frac{\partial \psi^i}{\partial y} + \mathrm{Ra}\left(\theta^i \frac{\partial N_k^i}{\partial x} + 2\gamma\theta^i N_k^i \frac{\partial N_k^i}{\partial x} + \phi^i \frac{\partial N_k^i}{\partial x}\right) \right) d\Omega$$

$$= \int_{\Gamma} N_k^i \left(\frac{\partial \psi^i}{\partial x} n_x + \frac{\partial \psi^i}{\partial y} n_y \right) d\Gamma_i + \int_{\Gamma} N_k^i n_x \theta^i d\Gamma_i \tag{33}$$

In obtaining Eq. (33), the Green's theorem is applied with respect to derivatives of ψ without affecting the θ terms. Using Eqs. (19, 20, 21) and (22) in (33), we have

$$\sum_m \psi_m^i \left\{ \int_{\Omega} \left((1 + M^2)\frac{\partial N_k^i}{\partial x}\frac{\partial N_m^i}{\partial x} + \frac{\partial N_m^i}{\partial y}\frac{\partial N_k^i}{\partial y} \right) d\Omega_i + \mathrm{Ra} \sum_L \left(\theta_L^i \int_{\Omega i} \mathrm{N_k^i} \frac{\partial N_L^i}{\partial x}(1 + 2\gamma N_{ki}^i) d\Omega + \phi_L^i N \int_{\Omega i} \mathrm{N_k^i} \frac{\partial N_L^i}{\partial x} d\Omega \right) \right\}$$

$$= \int_{\Gamma} N_k^i \left(\frac{\partial \psi^i}{\partial x} n_x + \frac{\partial \psi^i}{\partial y} n_y \right) d\Gamma_i + \int_{\Gamma} N_k^i \theta^i d\Omega_i = \Gamma_k^i \tag{34}$$

In the problem under consideration, for computational purpose, we choose uniform mesh of 10 triangular elements (Fig. II). The domain has vertices whose global coordinates are (0,0), (1,0) and (1,h) in the non-dimensional form. Let e_1, e_2…..e_{10} be the ten elements and let θ_1, θ_2,…..θ_{10} be the global values of θ and ψ_1, ψ_2,……ψ_{10} be the global values of ψ at the global nodes of the domain (Fig. II).

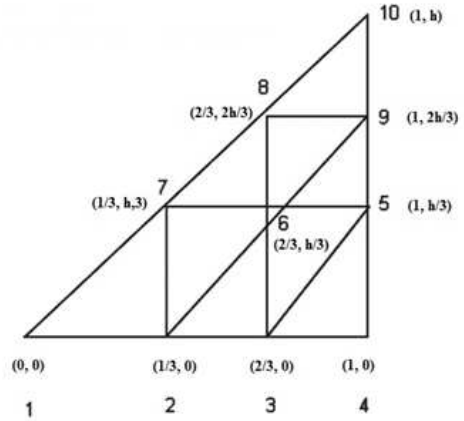

Fig. 2. Schematic Diagram of the Configuration

Shape Functions and Stiffness Matrices:

Range functions in $n_{i,j}$; i = element, j = node.

$$n_{1,1} = 1 - 3x, \quad n_{1,2} = 3x - \frac{3y}{h}, \quad n_{2,1} = 1 - \frac{3y}{h}, \quad n_{2,2} = -1 + \frac{3y}{h}, \quad n_{2,3} = 1 - 3x + \frac{3y}{h}, \quad n_{3,1} = 2 - 3x, \quad n_{3,2} = -1 + 3x - \frac{3y}{h}, \quad n_{3,3} = \frac{3y}{h}$$

$$n_{4,1} = 1 - \frac{3y}{h}, \quad n_{4,2} = -2 + 3x, \quad n_{4,3} = 2 - 3x + \frac{3y}{h}, \quad n_{5,1} = 2 - 3x, \quad n_{5,2} = -1 + 3x - \frac{3y}{h}, \quad n_{5,3} = \frac{3y}{h}, \quad n_{6,1} = 2 - 3x,$$

$$n_{6,2} = 3x - \frac{3y}{h} \quad n_{6,3} = 1 + \frac{3y}{h}, \quad n_{7,1} = 2 - \frac{3y}{h}, \quad n_{7,2} = -2 + 3x, \quad n_{7,3} = 1 - 3x + \frac{3y}{h}, \quad n_{8,1} = 3 - 3x, \quad n_{8,2} = -1 + 3x - \frac{3y}{h},$$

$$n_{9,2} = 3x - \frac{3y}{h}, \quad n_{9,3} = -1 + \frac{3y}{h}$$

Substituting the above shape functions in Eqs. (28), (29) and (34) with respect to each element and integrating over the respective triangular domain we obtain the element in the form Eq. (28). The 3x3 matrix equations are assembled using connectivity conditions to obtain a 8x8 matrix equations for the global nodes ψ_p,θ_p and ϕ_p.

The global matrix equation for θ is

$$A_3 X_3 = B_3 \tag{35}$$

The global matrix equation for ϕ is

$$A_4 X_4 = B_4 \tag{36}$$

The global matrix equation for ψ is

$$A_5 X_5 = B_5 \tag{37}$$

where

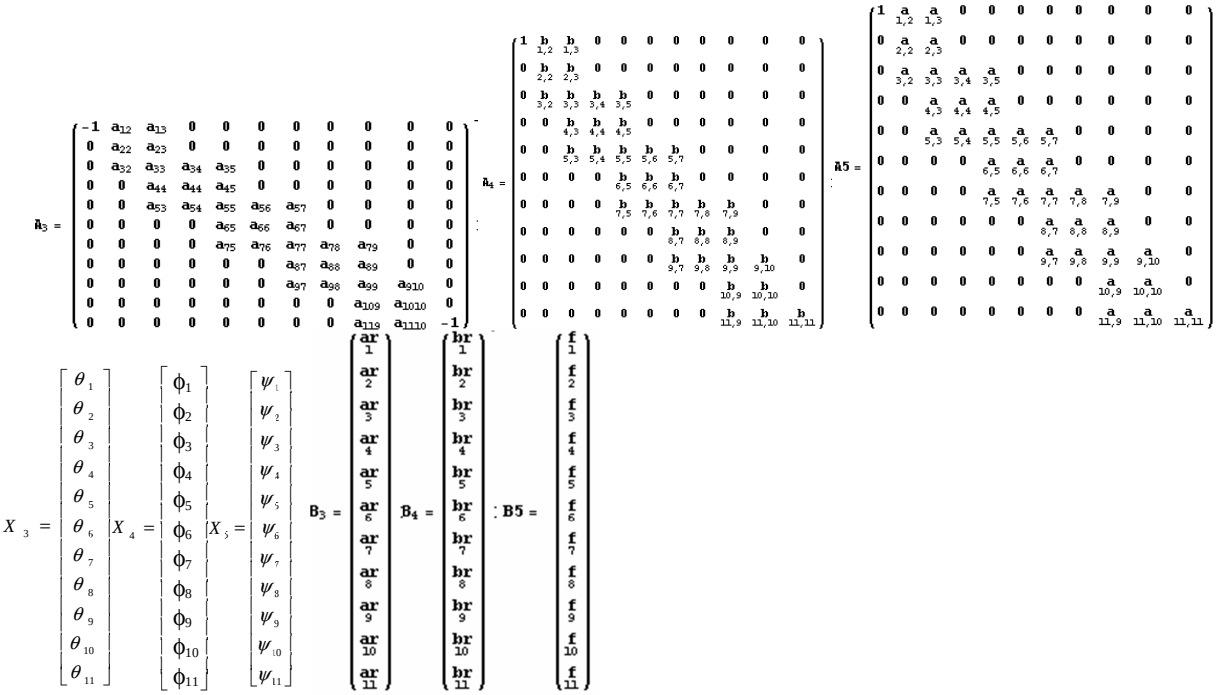

The global matrix equations are coupled and are solved under the following iterative procedures. At the beginning of the first iteration, the values of (ψ_i) are taken to be zero and the global equations (35) and (36) are solved for the nodal values of θ and ϕ. These obtained nodal values (θi) and (ϕi) are then used to solve the global equation (37) to obtain (ψ_i). In the second iteration, these (ψ_i) values are obtained and used in Eqs. (35) and (36) to calculate (θi) and (ϕi) and vice versa. The three equations are thus solved under iteration process until two consecutive iterations differ by a pre-assigned percentage.

The domain consists three horizontal levels and the solution for Ψ & θ at each level may be expressed in terms of the nodal values as follows:

In the horizontal strip $0 \le y \le \frac{h}{3}$

$$\Psi = (\Psi_1 N^1_1 + \Psi_2 N^1_2 + \Psi_7 N^1_7)\, H(1-\tau_1) = \Psi_1 (1-4x) + \Psi_2 4(x-\frac{y}{h}) + \Psi_7 (\frac{4y}{h}(1-\tau_1)) \qquad (0 \le x \le \frac{1}{3})$$

$$\Psi = (\Psi_2 N^3_2 + \Psi_3 N^3_3 + \Psi_6 N^3_6)\, H(1-\tau_2) + (\Psi_2 N^2_2 + \Psi_7 N^2_7 + \Psi_6 N^2_6) H(1-\tau_3) \qquad (\frac{1}{3} \le x \le \frac{2}{3})$$

$$= (\Psi_2 2(1-2x) + \Psi_3 (4x-\frac{4y}{h}-1) + \Psi_6 (\frac{4y}{h}))H(1-\tau_2) + (\Psi_2 (1-\frac{4y}{h}) + \Psi_7 (1+\frac{4y}{h}-4x) + \Psi_6 (4x-1))H(1-\tau_3)$$

$$\Psi = (\Psi_3 N^5_3 + \Psi_4 N^5_4 + \Psi_5 N^5_5)\, H(1-\tau_3) + (\Psi_3 N^4_3 + \Psi_5 N^4_5 + \Psi_6 N^4_6) H(1-\tau_4)$$

$$= (\Psi_3 (3-4x) + \Psi_4 2(2x-\frac{2y}{h}-1) + \Psi_6 (\frac{4y}{h}-4x+3))H(1-\tau_3) + \Psi_3 (1-\frac{4y}{h}) + \Psi_5 (4x-3) + \Psi_6 (\frac{4y}{h}))H(1-\tau_4) \qquad (\frac{2}{3} \le x \le 1)$$

Along the strip $\frac{h}{3} \le y \le \frac{2h}{3}$

$$\Psi = (\Psi_7 N^6_7 + \Psi_6 N^6_6 + \Psi_8 N^6_8)\, H(1-\tau_2) + (\Psi_6 N^7_6 + \Psi_9 N^7_9 + \Psi_8 N^7_8)\, H(1-\tau_3)$$

$$+ (\Psi_6 N^8_6 + \Psi_5 N^8_5 + \Psi_9 N^8_9)\, H(1-\tau_4) \qquad (\frac{1}{3} \le x \le 1)$$

$$\Psi = (\Psi_7 2(1-2x) + \Psi_6 (4x-3) + \Psi_8 (\frac{4y}{h}-1))H(1-\tau_3) + \Psi_6 (2(1-\frac{2y}{h}) + \Psi_9 (\frac{4y}{h}-1) + \Psi_8 (1+\frac{4y}{h}-4x))H(1-\tau_4)$$

$+ \Psi_6 (4(1-x)+ \Psi_5 (4x-\frac{4y}{h}-1)+ \Psi_9 2(\frac{2y}{h}-1))H(1-\tau_5)$

Along the strip $\frac{2h}{3} \le y \le 1$

$\Psi = (\Psi_8 N^9_8 + \Psi_9 N^9_9 + \Psi_{10} N^9_{10})\, H(1-\tau_6)$ $\quad (\frac{2}{3} \le x \le 1)$

$= \Psi_8 (4(1-x)+ \Psi_9 4(x-\frac{y}{h})+ \Psi_{10} 2(\frac{4y}{h}-3))H(1-\tau_6)$

where $\tau_1 = 4x$, $\tau_2 = 2x$, $\tau_3 = \frac{4x}{3}$, $\tau_4 = 4(x-\frac{y}{h})$, $\tau_5 = 2(x-\frac{y}{h})$, $\tau_6 = \frac{4}{3}(x-\frac{y}{h})$ and H represents the right side function.

The expressions for θ are as follows:

In the horizontal strip $0 \le y \le \frac{h}{3}$

$\theta = [\theta_1(1-4x)+ \theta_2\, 4(x-\frac{y}{h})+ \theta_7\ (\frac{4y}{h}))\, H(1-\tau_1)$ $\quad (0 \le x \le \frac{1}{3})$

$\theta = (\theta_2(2(1-2x)+ \theta_3\, (4x-\frac{4y}{h}-1)+ \theta_6(\frac{4y}{h}))\, H(1-\tau_2) + \theta_2(1-\frac{4y}{h})+ \theta_7(1+\frac{4y}{h}-4x)+ \theta_6(4x-1))H(1-\tau_3)$

$(\frac{1}{3} \le x \le \frac{2}{3})$

$\theta = \theta_3(3-4x) +2\, \theta_4(2x-\frac{2y}{h}-1)+ \theta_6(\frac{4y}{h}-4x+3)\, H(1-\tau_3) +(\theta_3(1-\frac{4y}{h})+ \theta_5(4x-3)+ \theta_6(\frac{4y}{h}))\, H(1-\tau_4)$

$(\frac{2}{3} \le x \le 1)$

Along the strip $\frac{h}{3} \le y \le \frac{2h}{3}$

$\theta = (\theta_7(2(1-2x)+ \theta_6(4x-3)+ \theta_8(\frac{4y}{h}-1))\, H(1-\tau_3) + (\theta_6(2(1-\frac{2y}{h})+ \theta_9(\frac{4y}{h}-1)+ \theta_8(1+\frac{4y}{h}-4x))\, H(1-\tau_4)$

$+ (\theta_6(4(1-x)+ \theta_5(4x-\frac{4y}{h}-1)+ \theta_9\, 2(\frac{4y}{h}-1))\, H(1-\tau_5)$ $\quad (\frac{1}{3} \le x \le \frac{2}{3})$

Along the strip $\frac{2h}{3} \le y \le 1$

$\theta = (\theta_8 4(1-x) + \theta_9 4(x-\frac{y}{h})+ \theta_{10}(\frac{4y}{h}-3)\, H(1-\tau_6)$ $\quad (\frac{2}{3} \le x \le 1)$

The expressions for ϕ are

$\phi = [\phi_1(1-4x)+ \phi_2\, 4(x-\frac{y}{h})+ \phi_7\ (\frac{4y}{h}))\, H(1-\tau_1)$ $\quad (0 \le x \le \frac{1}{3})$

$\phi = (\phi_2(2(1-2x)+ \phi_3\, (4x-\frac{4y}{h}-1)+ \phi_6(\frac{4y}{h}))\, H(1-\tau_2)$

$+ \phi_2(1-\frac{4y}{h})+ \phi_7(1+\frac{4y}{h}-4x)+ \phi_6(4x-1))H(1-\tau_3)$ $\quad (\frac{1}{3} \le x \le \frac{2}{3})$

$\phi = \phi_3(3-4x) +2\, \phi_4(2x-\frac{2y}{h}-1)+ \phi_6(\frac{4y}{h}-4x+3)\, H(1-\tau_3) + (\phi_3(1-\frac{4y}{h})+ \phi_5(4x-3)+ \phi_6(\frac{4y}{h}))\, H(1-\tau_4)$ $(\frac{2}{3} \le x \le 1)$

Along the strip $\frac{h}{3} \le y \le \frac{2h}{3}$

$\phi = (\phi_7(2(1-2x)+ \phi_6(4x-3)+ \phi_8(\frac{4y}{h}-1))\ H(1-\tau_3) + (\phi_6(2(1-\frac{2y}{h})+ \phi_9(\frac{4y}{h}-1)+ \phi_8(1+\frac{4y}{h}-4x))\ H(1-\tau_4)$

$+ (\phi_6(4(1-x)+ \phi_5(4x-\frac{4y}{h}-1)+ \phi_9\ 2(\frac{4y}{h}-1))\ H(1-\tau_5)$ $(\frac{1}{3}\le x\le\frac{2}{3})$

Along the strip $\frac{2h}{3}\le y\le 1$

$\phi = (\phi_8 4(1-x) + \phi_9 4(x-\frac{y}{h})+ \phi_{10}(\frac{4y}{h}-3)\ H(1-\tau_6)$ $(\frac{2}{3}\le x\le 1)$

The dimensionless Nusselt number (Nu) and the Sherwood number (Sh) on the non-insulated boundary walls of the rectangular duct are calculated using the formulas:

$Nu = (\frac{\partial\theta}{\partial x})_{x=1}$ and $Sh = (\frac{\partial\phi}{\partial x})_{x=1.}$

The Nusselt number on the side wall x=1 in different regions are given by

$$Nu_1 = \left(n_{5,1}\right)_x \theta_3 + \left(n_{5,2}\right)_x \theta_4 + \left(n_{5,3}\right)_x \theta_5 , Sh_1 = \left(n_{5,1}\right)_x \phi_3 + \left(n_{5,2}\right)_x \phi_4 + \left(n_{5,3}\right)_x \phi_5 , \quad (0 \le y \le h/3)$$

$$Nu_2 = \left(n_{6,1}\right)_x \theta_6 + \left(n_{6,2}\right)_x \theta_5 + \left(n_{6,3}\right)_x \theta_9 , Sh_2 = \left(n_{6,1}\right)_x \phi_6 + \left(n_{6,2}\right)_x \phi_5 + \left(n_{6,3}\right)_x \phi_9 \quad (h/3 \le y \le 2h/3)$$

$$Nu_3 = \left(n_{9,1}\right)_x \theta_8 + \left(n_{9,2}\right)_x \theta_9 + \left(n_{9,3}\right)_x \theta_{10} , Sh_3 = \left(n_{9,1}\right)_x \phi_8 + \left(n_{9,2}\right)_x \phi_9 + \left(n_{9,3}\right)_x \phi_{10} \quad (2h/3 \le y \le h)$$

The suffix ‘x’ denotes differentiation of the shape functions with respect to ‘x’. Substituting the shape functions and the boundary conditions, the Nusselt number and the Sherwood number in different regions are

$Nu_1=2-4\theta_3$ $(0 \le y \le h/3)$, $Nu_2=2-4\theta_5$ $(h/3 \le y \le 2h/3)$, $Nu_3=2-4\theta_7$ $(2h/3 \le y \le h)$

The Sherwood number on the side wall x=1 in different regions are:

$Sh_1=2-4\phi_3$ $(0 \le y \le h/3)$, $Sh_2=2-4\phi_5$ $(h/3 \le y \le 2h/3)$, $Sh_3=2-4\phi_7$ $(2h/3 \le y \le h)$

Comparison:

In this analysis, it should be mentioned that the results obtained herein are compared with the results of Shanthi *et al.* [13] as shown in Table A in the absence of Du=0, γ=0, Q=0 and the results are found to be in good agreement.

Table A. Comparison of the present results (Du = 0, γ= 0, k=0) with Shanthi et al. [13] results

Present results							
N	1	2	-0.5	-0.8	1	2	3
S_0	0.5	0.5	0.5	0.5	1	1.5	2
Nu_1	61.12512	52.523	10.1212	9.8676	62.5249	64.1294	66.13432
Nu_2	58.16134	51.1356	11.16545	9.85643	59.1264	60.1965	61.8965
Nu_3	54.49213	50.2023	11.7932	9.8543	55.0982	56.2892	57.38112
Sh_1	21.9445	20.4345	3.379233	4.13521	15.42534	13.1262	11.8964
Sh_2	26.516	21.1163	4.69311	5.17923	11.16923	19.0562	18.8093
Sh_3	19.0922	29.7002	6.0722	6.23123	18.1762	17.0691	16.1242

Shanthi et al. [13] results							
N	1	2	-0.5	-0.8	1	2	3
S_0	0.5	0.5	0.5	0.5	1	1.5	2
Nu_1	61.1251	52.523	10.214	9.867	62.524	64.129	66.134
Nu_2	58.161	51.135	11.165	9.856	59.126	60.196	61.896
Nu_3	54.492	50.202	11.793	9.854	55.098	56.289	57.381
Sh_1	21.944	20.43	3.3792	4.135	15.425	13.126	11.896
Sh_2	26.516	21.116	4.693	5.1792	11.169	19.056	18.809
Sh_3	19.092	29.7	6.0072	6.231	18.176	17.069	16.124

RESULTS AND DISCUSSION

In this analysis, we investigate the effect of the non-linear density temperature variation in a convective heat and mass transfer of an electrically-conducting viscous fluid through a porous medium in a rectangular duct with Soret and Dufour effects. The equations governing the flow and heat and mass transfer have been solved by employing the Galerkin finite-element analysis with tri-nodal triangular elements. The non-dimensional temperature (θ) is shown in Figs. 3-22 for different values of M, Q, Rad, So, Du and γ at different horizontal and vertical levels. The temperature

(θ) and concentration (ϕ) are plotted versus different levels of x and y for the values M=5, N= 1, α=2, k=0.5, Q=0.5, Rad=0.05, Sr=2, Du=0.3, Pr=0.71, N=0.5, γ=0.01, Ra=0.5 and specific variations of physical parametric values varies unless remain same. We follow the convention that the non-dimensional temperature θ is positive or negative according to whether the actual temperate (T) is greater or less than the temperature (T_c) on the cold wall x=1.

2.1. Temperature Profiles

Figs. 3-6 present θ with the Hartmann number M. We find that the higher the Lorentz force the larger the actual temperature at y=h/3 and the vertical levels x=1/3 and 2/3 and reduces at the higher horizontal level y=2h/3. This is due to the fact that the strength of flow decreases and thereby the temperature enhances in the boundary layer. Figs. 7-10 present θ with the radiation absorption parameter Q. It is observed that an increase in Q, enhances the actual temperature at y=h/3, and x=1/3 and 2/3 levels and reduces at y=2h/3 level. As the Rosseland radiative absorption parameter Q diminishes, the subsequent heat flux varies and thus reduces the rate of radiative heat transfer to the fluid which causes the rise in temperature. Figs. 11-14 display θ with the radiation parameter Rad. It is found that the higher the thermal radiation the smaller the actual temperature at both the vertical levels and at y=2h/3 level and larger at y=h/3 level. This may be due to the thermal radiation increases gradually in the fluid flow, causes an enhancement in the temperature in the boundary layer of the fluid flow. Figs. 15-18 show θ with the Soret parameter So or the Dufour parameter Du. By increasing the value of So (or decreasing Du), we notice an enhancement in the actual temperature at y=2h/3 level, and depreciation at y=h/3, x=1/3 and 2/3 levels. This is attributed to the fact that an enhancement of Soret parameter So (or decrease in Dufour parameter Daf) results an increase in the thickness of the boundary layer at the upper levels and reduces at lower levels of the fluid. The effect of the non–linear density temperature relation on θ is executed in Figs. 19-22. It is found that the actual temperature enhances at y=h/3, x=1/3 and 2/3 levels, while at y=2h/3 level, the actual temperature reduces with γ ≤0.5 and enhances with γ ≥0.7. This is due to fact that the thickness of the boundary layer flow reduces and results the enhancement in the temperature at horizontal levels of the boundary layer and reduces the temperature for vertical levels of the boundary layer flow.

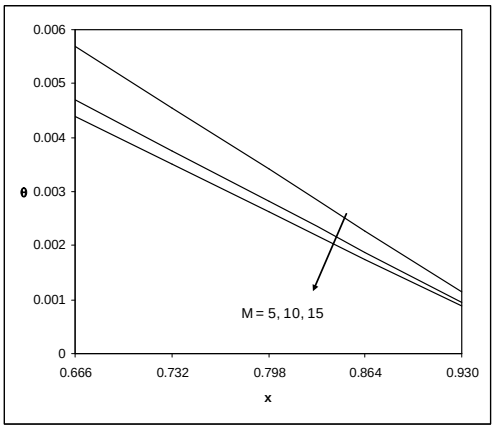

Fig. 3 : Variation of θ with M at $y=\frac{2h}{3}$ level

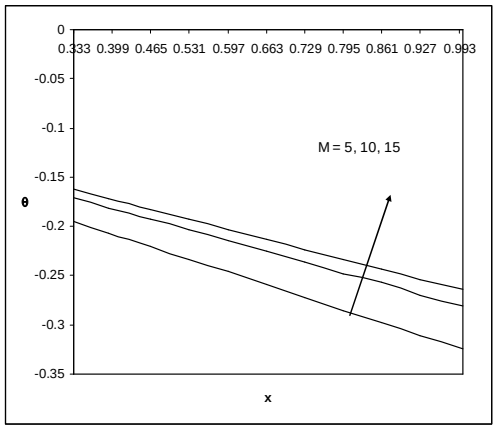

Fig. 4 : Variation of θ with M at $y=\frac{h}{3}$ level

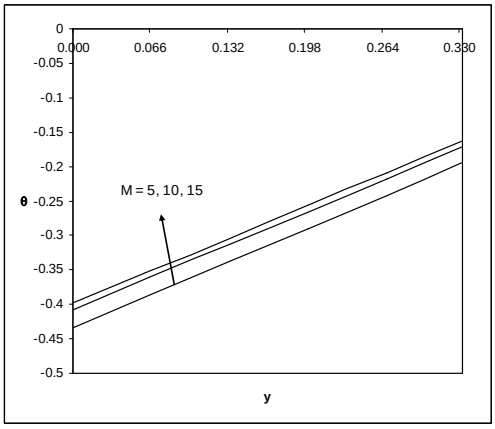

Fig. 5 : Variation of θ with M at $x=\frac{1}{3}$ level

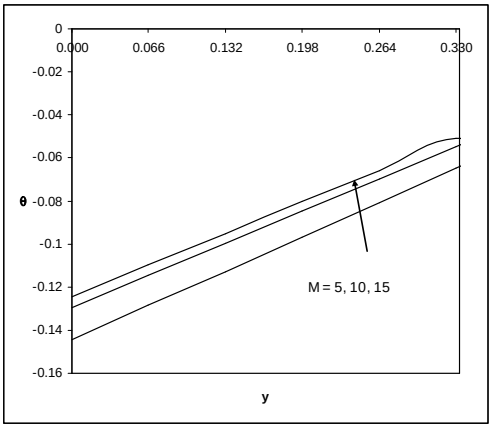

Fig. 6 : Variation of θ with M at $x=\frac{2}{3}$ level

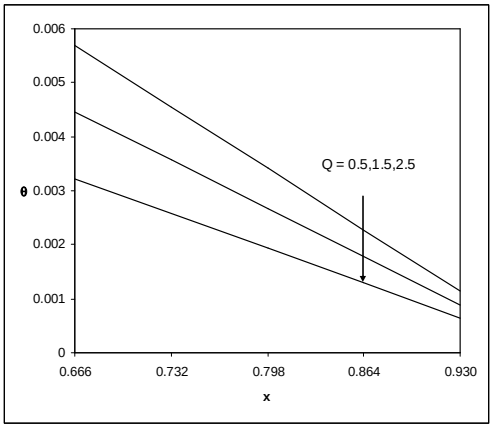

Fig. 7 : Variation of θ with Q at $y = \frac{2h}{3}$ level

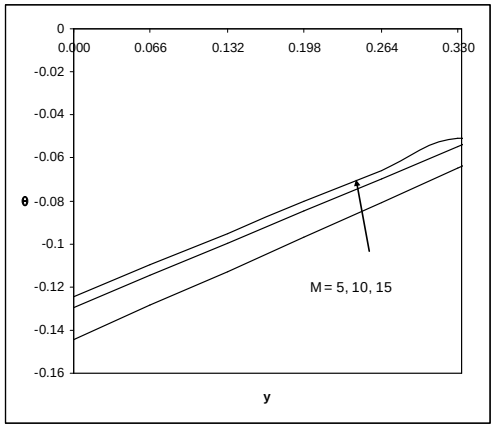

Fig. 8 : Variation of θ with Q at $y = \frac{h}{3}$ level

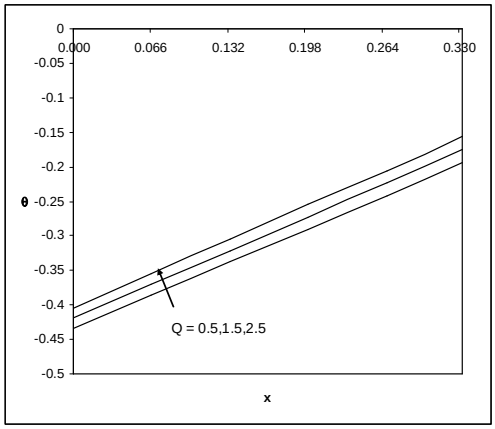

Fig. 9 : Variation of θ with Q at $x = \frac{1}{3}$ level

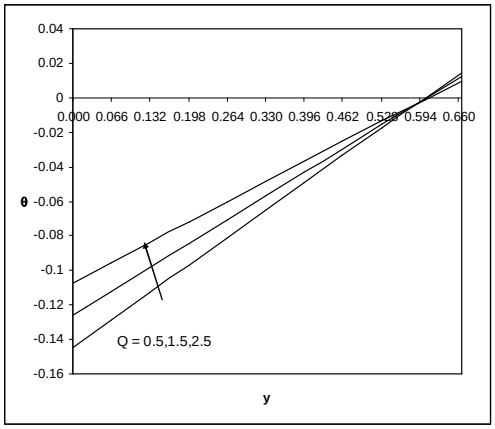

Fig. 10 : Variation of θ with Q at $x = \frac{2}{3}$ level

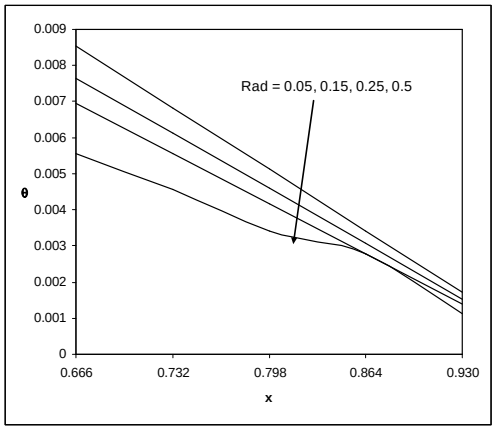

Fig. 11: Variation of θ with Rad at $y = \frac{2h}{3}$ level

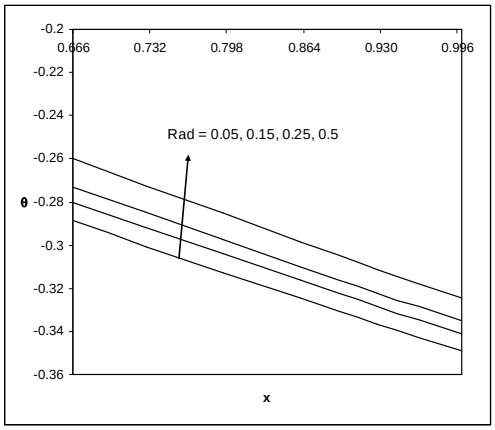

Fig. 12 : Variation of θ with Rad at $y = \frac{h}{3}$ level

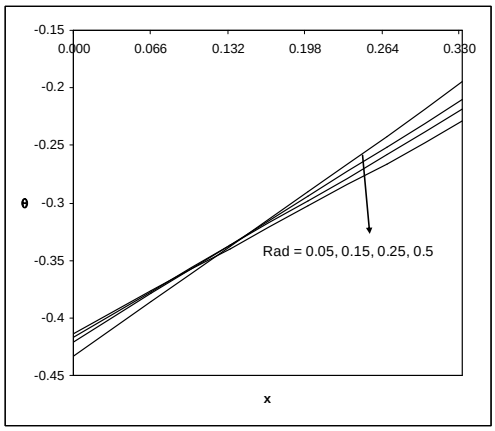

Fig. 13 : Variation of θ with Rad at $x = \frac{1}{3}$ level

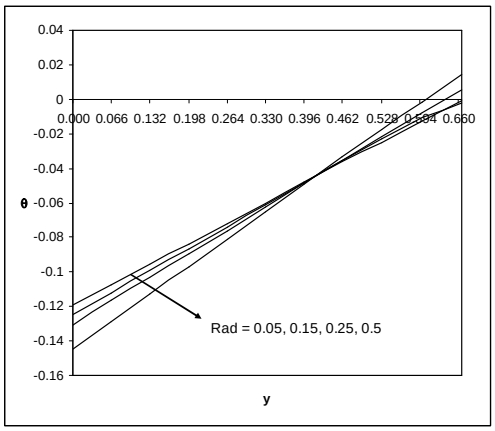

Fig. 14 : Variation of θ with Rad at $x = \frac{2}{3}$ level

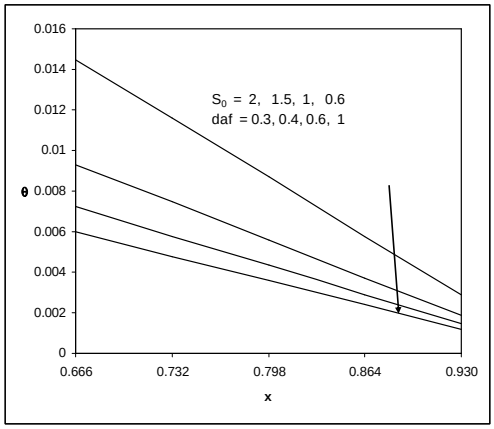

Fig. 15 : Variation of θ with S_0 & daf at $y = \frac{2h}{3}$ level

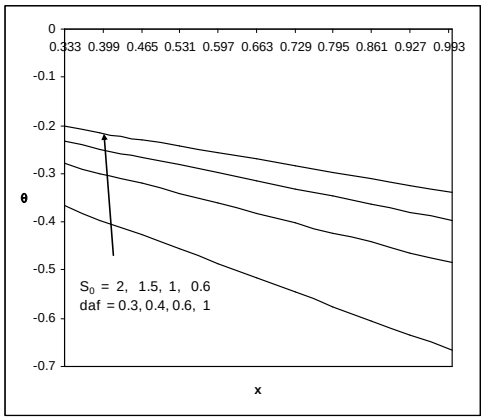

Fig. 16 : Variation of θ with S_0 & daf at $y = \frac{h}{3}$ level

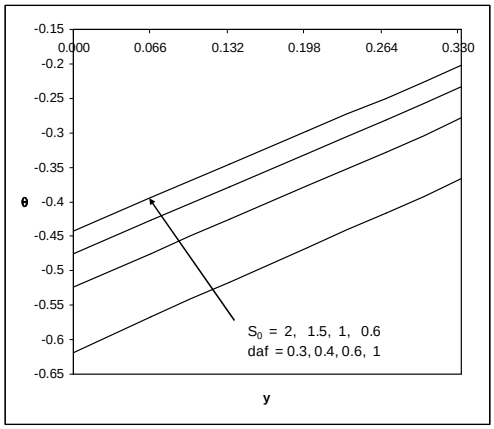

Fig. 17 : Variation of θ with S_0 & daf at $x = \frac{1}{3}$ level

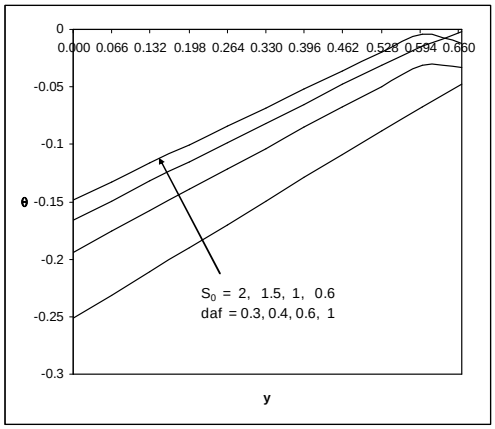

Fig. 18 : Variation of θ with S_0 & daf at $x = \frac{2}{3}$ level

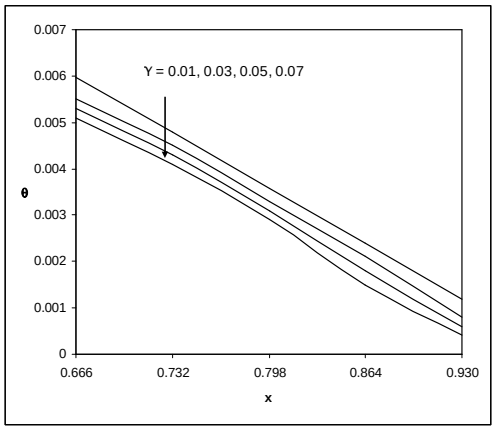

Fig. 19 : Variation of θ with γ at $y = \frac{2h}{3}$ level

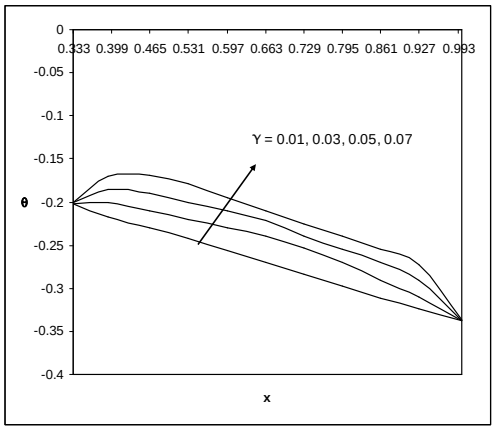

Fig. 20 : Variation of θ with γ at $y = \frac{h}{3}$ level

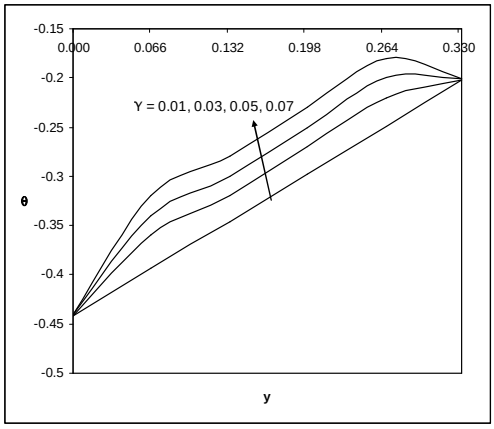

Fig. 21 : Variation of θ with γ at $x = \frac{1}{3}$ level

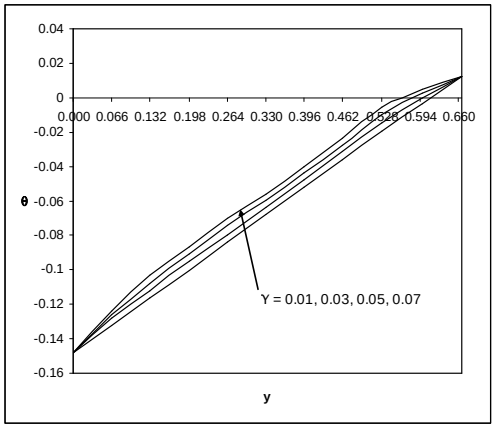

Fig. 22 : Variation of θ with γ at $x = \frac{2}{3}$ level

2.2. Concentration Profiles

The concentration distribution (C) is shown in Figs. 23-42 for different parametric values at different horizontal and vertical levels. We follow the convention that the concentration is positive or negative according to whether the actual concentration is greater or less than C_c, the concentration on the cold wall. Figs. 23-26 present C with M. It is found that the Lorentz force reduces the actual concentration and for further lowering of the force smaller the actual concentration at the levels y=h/3, 2h/3, x=1/3, 2/3. This is due to the fact that the strength of flow decreases and thereby the concentration reduces in the flow region Figs. 27-30 show C with Q. An increase in the radiation absorption parameter Q, reduces the actual concentration at y=2h/3 level and enhances it at y=h/3 and x=1/3 levels. At x=2/3 level, the actual concentration enhances in the region (0.066, 0.33) and reduces in the flow region (0.396, 0.666). As the radiation absorption increases in the entire flow region the actual concentration increase in the boundary layer fluid and decrease at the horizontal levels. Figs. 31-34 show the variation of C with the thermal radiation parameter Rad. It is found that the actual concentration reduces with Rad at y=2h/3 and x=1/3 and 2/3 levels and enhances at y=h/3 level. This may be due to the thermal radiation increases gradually in the fluid flow, causes depreciation in the concentration in the higher levels and enhances in the lower levels of the fluid flow. Figs. 35-38 display C with So and Daf. It can be seen from the profiles that increasing So (or decreasing Daf) results in an enhancement in the actual concentration at y=2h/3 and depreciation at y=h/3 and x=1/3 levels (Figs. 36-37). This is due to the fact that an enhancement of Soret parameter So (or decrease in Dufour parameter Daf) results an increase in the thickness of the boundary layer at the upper levels and reduces at lower level of the fluid. At x=2/3 level, the actual concentration reduces in the horizontal strip ($0 \le y \le 0.264$) and enhances in the region ($0.33 \le y \le 0.666$) for $So \le 1.5$ and for $So \ge 2$, we found a depreciation in the actual concentration in the entire region as shown in Fig. 38. Figs. 39-42 show the variation of C with the density ratio γ. The thickness of the boundary layer flow reduces due to the enhancement of concentration in the entire flow region. It can be seen from the profiles that the non-linearity in the density-temperature relation results in depreciation in the actual concentration at all levels.

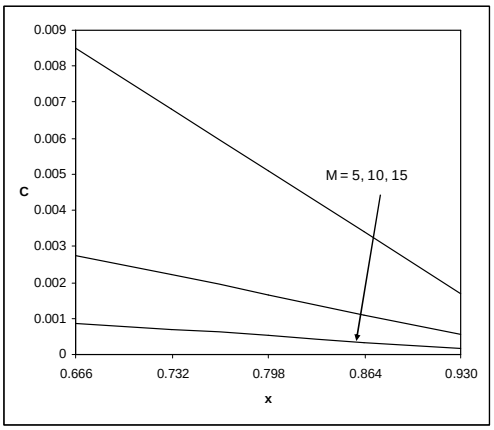

Fig. 23 : Variation of C with M at $y = \frac{2h}{3}$ level

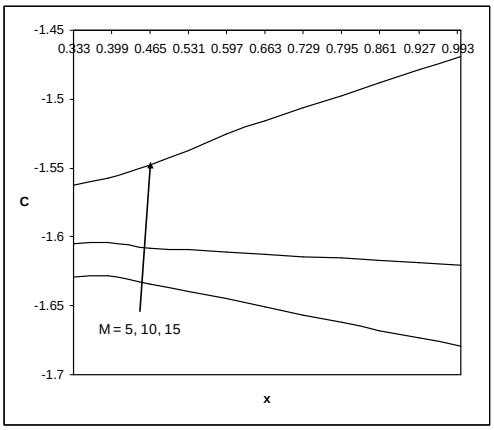

Fig. 24 : Variation of C with M at $y = \frac{h}{3}$ level

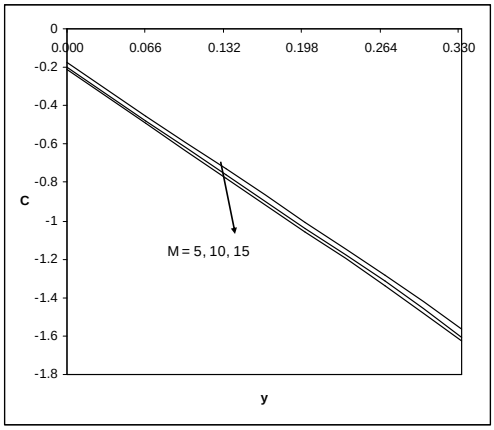

Fig. 25 : Variation of C with M at $x = \frac{1}{3}$ level

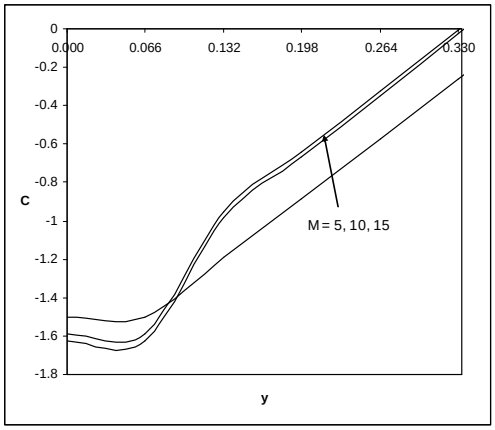

Fig. 26 : Variation of C with M at $x = \frac{2}{3}$ level

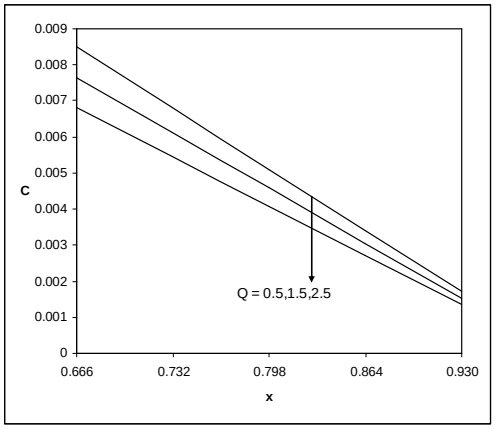

Fig. 27 : Variation of C with Q at $y = \frac{2h}{3}$ level

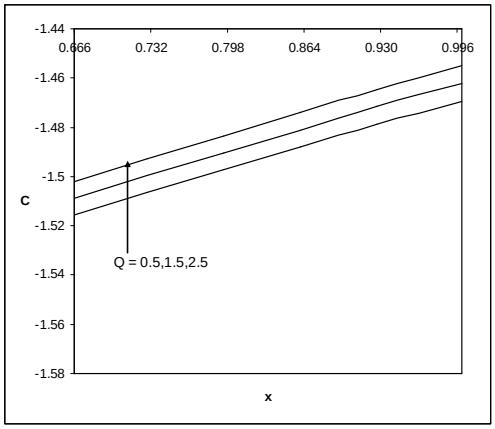

Fig. 28 : Variation of C with Q at $y = \frac{h}{3}$ level

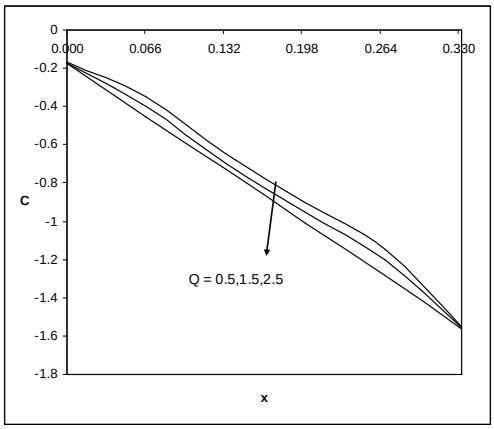

Fig. 29 : Variation of C with Q at $x = \frac{1}{3}$ level

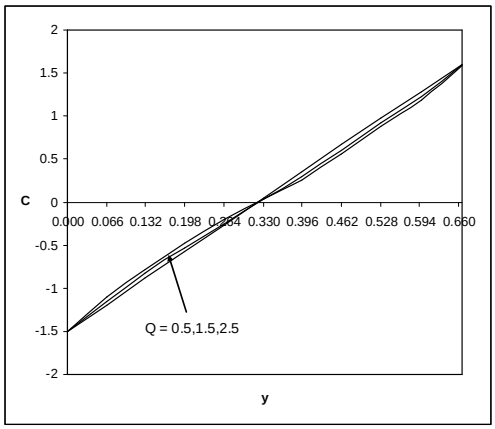

Fig. 30 : Variation of C with Q at $x = \frac{2}{3}$ level

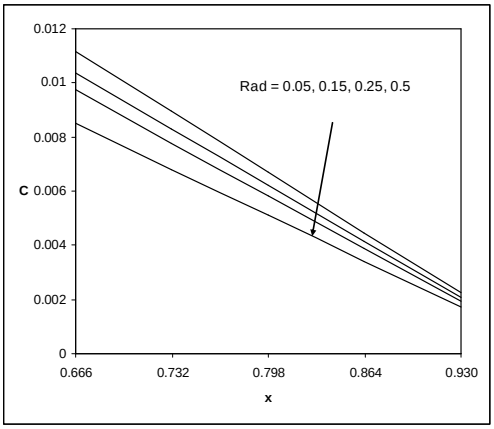

Fig. 31: Variation of C with Rad at $y = \frac{2h}{3}$ level

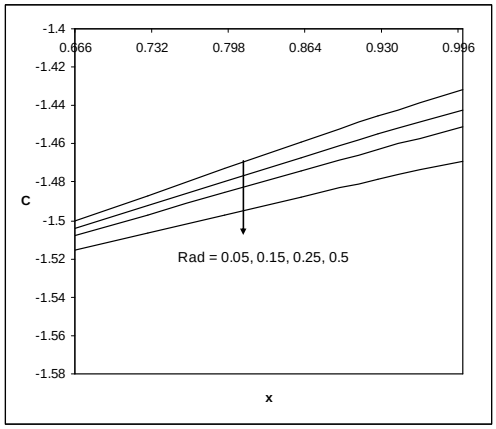

Fig. 32 : Variation of C with Rad at $y = \frac{h}{3}$ level

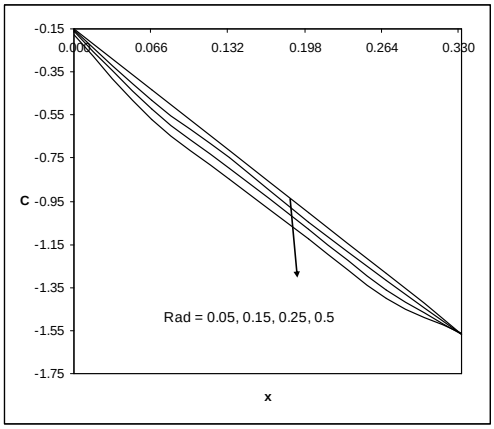

Fig. 33 : Variation of C with Rad at $x = \frac{1}{3}$ level

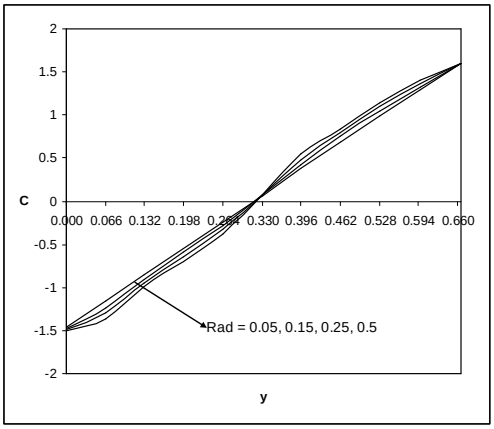

Fig. 34 : Variation of C with Rad at $x = \frac{2}{3}$ level

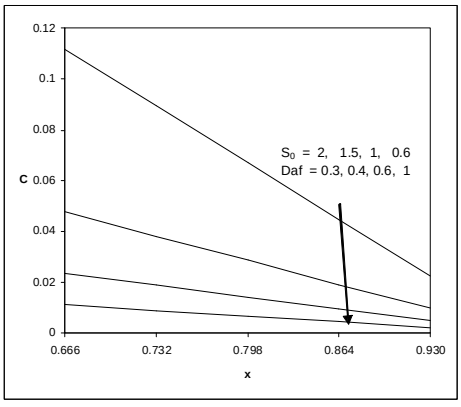

Fig. 35 : Variation of C with S_0 & Daf at $y = \frac{2h}{3}$ level

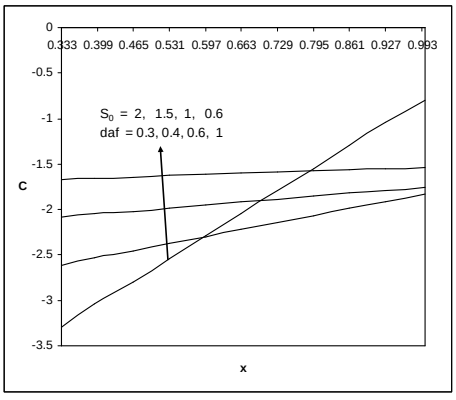

Fig. 36 : Variation of C with S_0 & Daf at $y = \frac{h}{3}$ level

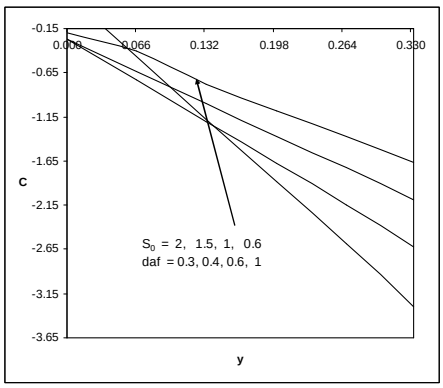

Fig. 37 : Variation of C with S_0 & Daf at $x=\frac{1}{3}$ level

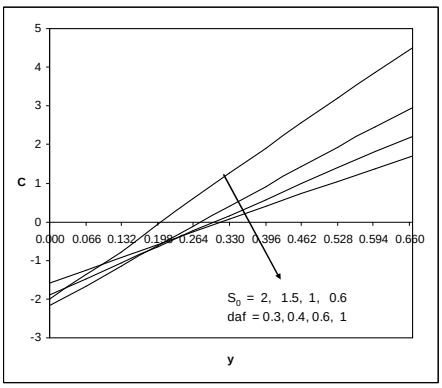

Fig. 38 : Variation of C with S_0 & Daf at $x=\frac{2}{3}$ level

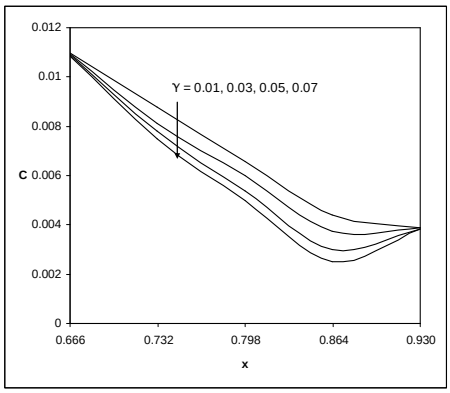

Fig. 39 : Variation of C with γ at $y=\frac{2h}{3}$ level

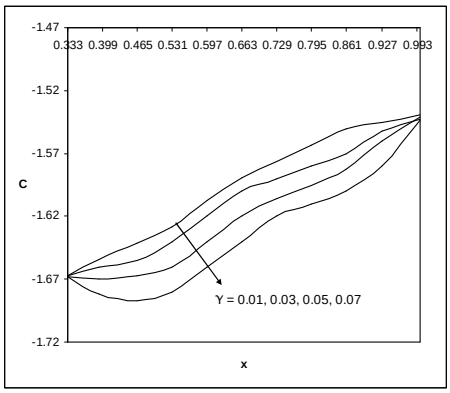

Fig. 40 : Variation of C with γ at $y=\frac{h}{3}$ level

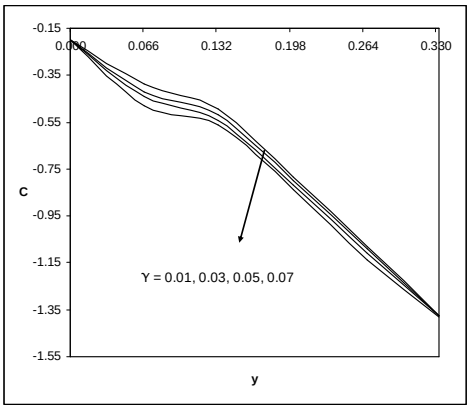

Fig. 41 : Variation of C with γ at $x=\frac{1}{3}$ level

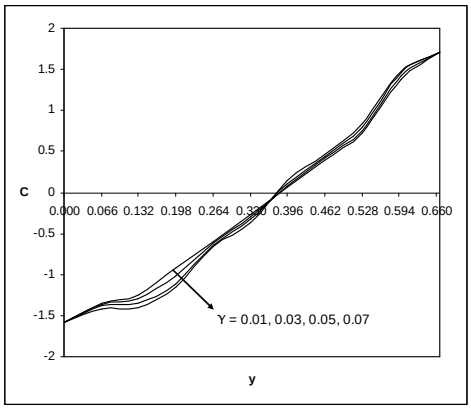

Fig. 42 : Variation of C with γ at $x=\frac{2}{3}$ level

The rate of heat transfer, Nusselt number (Nu) and the rate of mass transfer, Sherwood number (Sh), on the side x=1 are shown in Tables 1-5 for different values of M, Q, Rad, So, Du and Υ. With respect to the Hartmann number M, we find that the higher the molecular diffusivity, the smaller $|Nu|$ on the lower quadrant and larger on the middle and upper quadrants and for further higher Lorentz force the larger $|Nu|$ on the lower quadrant and smaller on the middle and upper quadrant. An increase in M, enhances $|Sh|$ on the lower and middle quadrants and reduces it on the upper quadrant. $|Sh|$ experiences depreciation with an increase in Q on all the three quadrants as shown in Table 1.

Table 1: Effect of M on Nusselt and Sherwood numbers for Q=0.5, Rad=0.05, So=2, Du=0.3, γ=0.01, X=1

Parameter M	Nu1	Nu2	Nu3	Sh1	Sh2	Sh3
5	2.5720	2.2538	1.9356	6.84148	1.57600	-3.68944
10	1.6655	2.6081	3.5617	8.35244	2.03041	-4.2916
15	1.8391	2.2948	2.7505	8.49364	2.11208	-4.26948

An increase in the radiation absorption parameter Q, reduces │Nu│ on the lower and middle quadrants and enhances it on the upper quadrant. │Sh│ experiences depreciation with an increase in Q on all the three quadrants as shown in Table 2.

Table 2: Effect of Q on Nusselt and Sherwood numbers for M=0.5, Rad=0.05, So=2, Du=0.3, γ =0.01, X=1

Parameter Q	Nu1	Nu2	Nu3	Sh1	Sh2	Sh3
0.5	1.8391	2.2948	2.7505	8.4937	2.1121	-4.2695
1.5	2.5030	2.2269	1.9509	7.9952	1.8123	-4.3699
2.5	2.4288	2.1947	1.9607	7.981	1.8113	-4.3584

The variation of Nu with Radiation parameter Rad shows that the Nusselt number enhances on the lower quadrant and reduces on the upper quadrant with an increase in Rad, while on the middle quadrant, the Nusselt number reduces for the condition Rad≤0.5 and enhances for Rad ≥ 1.5. With respect to the radiation parameter Rad, we find that the rate of mass transfer on the lower and middle quadrants reduces for Rad≤0.5 and enhances for Rad ≥2.5 while in the upper quadrant it reduces with Rad. The variation of Sh with the buoyancy ratio of N shows that │Sh│ reduces on all the three quadrants with an increase in N≥ 0 while the buoyancy forces are in the same direction and for the forces acting in the opposite direction the Sherwood number on the lower and middle quadrants enhances with │Rad│ and reduces on the upper quadrant as shown in Table 3.

Table 3: Effect of Rad on Nusselt and Sherwood numbers for M=0.5, Q=0.5, So=2, Du=0.3, γ =0.01, X=1

Parameter Rad	Nu1	Nu2	Nu3	Sh1	Sh2	Sh3
0.05	-1.510	7.506	16.522	6.3046	0.3478	-5.609
0.15	7.893	1.749	-4.393	7.8725	1.7499	-4.394
0.25	7.931	0.365	-4.387	7.9311	1.7717	-4.388
0.5	8.009	0.574	-4.381	8.0092	2.5848	-4.382

The variation of Nu with the Soret and Dufour parameters (So and Du) are shown in Table 4. An increase in the Soret parameter So≤1.5 (or a decrease in the Dufour parameter Du) enhances │Nu│ and reduces for So≥2.0 on all the three quadrants. With respect to the Soret and Dufour parameters (So and Du), we find that increasing So (So≥1.5) (or decreasing Du) enhances Sh on the lower quadrant, and reduces in the upper quadrant and for So≥2, we notice a depreciation in │Sh│ on the lower quadrant and an enhancement on the upper quadrant. │Sh│ reduces with So in the lower and middle quadrants.

Table 4: Effect of So, Du on Nusselt and Sherwood numbers for M=0.5, Q=0.5, Rad=0.05, γ =0.01, X=1

Parameter So, Du	Nu1	Nu2	Nu3	Sh1	Sh2	Sh3
2,0.3	2.5022	2.2709	2.0502	8.3344	1.7415	-4.8514
1.5,0.4	3.7744	3.4242	3.0653	8.6888	1.34842	-3.8328
1,0.6	3.6641	3.3475	3.2989	7.3489	1.28483	-3.962
0.6,1	3.5930	3.2870	3.0671	7.2432	1.2678	-4.851

The variation of Nu with the density ratio ϒ shows that the Nusselt number reduces with ϒ on the lower quadrant while on the middle and the upper quadrants │Nu│ reduces with ϒ≤0.5 and enhances for ϒ≥0.7. The variation of Sh with the density ratio ϒ shows that │Sh│ enhances on the lower and middle quadrants with an increase in ϒ, while in the upper quadrant, it reduces for ϒ≤ 0.03 and enhances for ϒ≤0.05 as shown in Table 5.

Table 5: Effect of γ on Nusselt and Sherwood numbers for M=0.5, Q=0.5, Rad=0.05, So=2, Du=0.3, X=1

Parameter γ	Nu1	Nu2	Nu3	Sh1	Sh2	Sh3
0.01	2.5939	2.2079	1.9507	8.3344	1.7415	-4.8514
0.03	2.5934	2.2076	1.9504	8.3388	1.7443	2.5008
0.05	2.5928	2.2714	1.9501	8.3432	1.7472	-4.8487
0.07	2.5022	2.2719	2.0502	8.3476	1.7501	-4.8493

CONCLUSION

The problem of mixed convective flow of a viscous electrically-conducting fluid through a porous medium in a rectangular duct in the presence of Soret and Dufour effects was investigated. The equations were solved numerically using the Galerkin finite-element analysis with tri-nodal triangular elements for the computation of the flow, heat and mass transfer characteristics for various values of the Hartmann number, strength of heat source, radiation parameter, Soret number, Dufour number and the density ratio. We considered the heat flux on the base and the top walls to be constant. We assumed that the convective fluid and the porous medium were everywhere in local thermal equilibrium and that there was no phase change of the fluid in the medium. The properties of the fluid

and the porous medium were assumed homogeneous and isotropic, and the porous medium was assumed to be closely packed so that the Darcy's momentum law was adequate in the porous medium. The numerical results were obtained and compared with previously reported cases available in the open literature and they were found to be in good agreement. Graphical results for various parametric conditions were presented and discussed for different values. The main findings are summarized as follows:

- The presence of the Magnetic field M caused a significant effect on the heat and mass transfer rates.
- An increase in Radiation absorption parameter Q the actual temperature and actual concentration enhances at vertical level. However, the actual temperature and actual concentration decreases at horizontal levels.
- At higher values of Thermal radiation parameter Rad, smaller the actual temperature at both vertical levels and at y=2h/3 and larger at y=h/3. Furthermore, the actual temperature and actual concentration decreases at the horizontal levels.
- An increase in Soret parameter So (or decrease in Dufour parameter Du) increases the actual temperature and actual concentration at vertical levels. An increase in Soret parameter So (or decrease in Dufour parameter Du) reduces the actual temperature and actual concentration at horizontal levels.
- Presence of Non-linear-Density-temperature relation (ϒ) influences the actual temperature at both vertical and horizontal levels. While the Non-linear-Density-Temperature relation results depreciation in the actual concentration at all levels.

REFERENCES

[1] S. Ostrach, H.D. Jiang, Y. Kamotani. In: ASME–JSME Thermal Engineering Joint Conference, Hawaii, (**1987**).
[2] R. Viskanta, T.L. Bergman, F.P. Incropera, Double-diffusive natural convection, In: S. Kakac, W. Aung, R. Viskanta (Eds.), Natural Convection: Fundamentals and Applications, Hemisphere, Washington, DC (**1985**) 1075–1099.
[3] A. Bejan, *Int. J. Heat Fluid Flow*, **1985**, 6, 149–159.
[4] Y. Kamotani, L.W. Wang, S. Ostrach, H.D. Jiang, *Int. J. Heat Mass Transfer*, **1985**, 28, 165–173.
[5] J.W. Lee, J.M. Hyun, *Int. J. Heat Mass Transfer*, **1990**, 33, 1619–1632.
[6] J. Lee, M.T. Hyun, K.W. Kim, *Int. J. Heat Mass Transfer*, **1988**, 31, 1969–1977.
[7] P. Ranganatha, R. Viskanta. In: ASME-JSME Thermal Engineering Joint Conference, Hawaii (**1987**).
[8] O.V. Trevisan, A. Bejan, *Int. J. Heat Mass Transfer*, **1986**, 29, 403–415.
[9] C. Beghein, F. Haghighat, F. Allard, *Int. J. Heat Mass Transfer*, **1992**, 35, 833–846.
[10] T. Nishimura, M. Wakamatsu, A.M. Morega, *Int. J. Heat Mass Transfer*, **1998**, 4l, 1601–1611.
[11] S. Sivaiah, Ph.D Thesis, S.K. University, (AP, India **2004**).
[12] A.J. Chamkha, H. Al-Naser, *Int. J. of Heat and Mass Transfer*, **2002**, 45, 2465-2483.
[13] G. Shanthi, S. Jafarunnisa, D.R.V. Prasada Rao, *Int. J. Electrical, Electronics and Computing Tech.*, **2011**, 2(4), 29-34.
[14] Al-Farhany, K.A. Turan, *Int. Commun. Heat and Mass Transfer*, **2012**, 39 (2), 174-181.
[15] G.M. Oreper, J. Szekely, *J. Cryst. Growth*, **1983**, 64, 505–515.
[16] H. Ozoe, M. Maruo, *JSME*, **1987**, 30, 774–778.
[17] J.P. Garandet, T. Alboussiere, R. Moreau, *Int. J. Heat Mass Transfer*, **1992**, 35, 741–748.
[18] S. Alchaar, P. Vasseur, E. Bilgen, ASME *J. Heat Transfer*, **1995**, 117, 668–673.
[19] N. Rudraiah, R.M. Barron, M. Venkatachalappa, C.K. Subbaraya, *Int. J. Eng. Sci*., **1995**, 33 1075–1084.
[20] N.M. Al-Najem, K.M. Khanafer, M.M. El-Refaee, *Int. J. Numer. Methods Heat Fluid Flow*, **1998**, 8, 651–672.
[21] P.X. Yu, J.X. Qiu, Q. Qin, Zhen F. Tian, *Int. J. Heat Mass Transfer*, **2013**, 67, 1131-1144.
[22] S. Acharya, R.J. Goldstein, *ASME J. Heat Transfer*, **1985**, 107, 855–866.
[23] A.G. Churbanov, P.N. Vabishchevich, V.V. Chudanov, V.F. Strizhov, *Int. J. Heat and Mass Transfer*, **1994**, 37, 2969–2984.
[24] K. Vajravelu, J. Nayfeh, *Int. Commun. Heat Mass Transfer*, **1992**, 19, 701–710.
[25] A.J. Chamkha, *Numer. Heat Transfer*, **1997**, Part A, 32, 653–675.
[26] T. Grosan, C. Revnic, I. Pop, D.B.Ingham, Int. J. Heat Mass Transfer, **2009**, 52, 1525-1533.
[27] B.V.K. Reddy, A. Narasimhan, *Int. Commun. Heat Mass Transfer*, **2010**, 37, 607-610.
[28] N.A.Baker, A.Karimipour, R.Roslan, *J. Thermodynamics*, **2016**, Article ID 3487182, http://dx.doi.org/10.1155/2016/3487182.
[29] J.D. Verschoor, P. Greebler, *Am. Soc. Mech. Engrs.*, **1952**, 961-968.
[30] A. Barletta, B. Pulvirenti, *Int. J. Heat and Mass Transfer*, **2000**, 43(5), 725-740.
[31] J. Van Rij, T. Ameel, T. Harman, Int. J. Thermal Sciences, **2009**, 48(2), 271281.
[32] A. Padmavathi, *Jour. Phys and Appl. Phys*, **2009**, 2.
[33] V. Nagaradhika, Y. Gayatri, D.R.V. Prasada Rao, Ajay Vasista, *Int. Jour. Electrical Electronics and Computing Tech.*, **2011**, 2(4), 1098-117.

[34] G. Sreenivasa, Ph.D. Thesis, S.K. University, (AP, India **2005**).
[35] J.C. Umavathi, Odelu Ojjela, *Int. J. Heat and Mass Transfer*, **2015**, 84, 1-15.
[36] J.C. Umavathi, M.A. Sheremet, *Int. J. Non-Linear Mechanics*, **2016**, 78, 17-28.
[37] O.D.Makinde, *Int. Commun. Heat Mass Transfer*, **2005**, 32(10), 1411-1419.
[38] H.C. Chiu, J.H. Jang, W.M. Yan, *Int. J. Heat and Mass Transfer*, **2007**, 50, 15-16, 2874-2882.
[39] A. Sakurai, K. Matsubara, K. Takakuwa, R. Kanbayashi, *Int. J Heat and Mass Transfer*, **2012**, 55, 2539-2548.
[40] T.R. Mahapatra, Dulal Pal, S. Mondal, *Int. Commun. Heat Mass Transfer*, **2013**, 41, 47-56.
[41] J. Lee, D. Jo, H. Chae, S.H. Chang, Y.H. Jeong, J.J. Jeong, *Experimental Thermal and Fluid Science*, **2015**, 69, 86-98.
[42] X. Liu, L. Wang, Z.M. Zhang, *Nanoscale and Microscale Thermophysical Engineering*, **2015**, 19(2), 98-126.
[43] M. Sheikholeslami, T. Hayat, A. Alsaedi, *Int. J Heat and Mass Transfer*, **2016**, 96, 513-524.
[44] C.Y. Cheng, *Int. Commun. Heat and Mass Transfer*, **2011**, *38 (1), 44-48.*
[45] A.J. Chamkha, M.M. Abd El-Aziz, and S.*E. Ahmed, Progress in Computational Fluid Dynamics*, **2012**, 12, 400-414.
[46] M. Motozawa, J. Chang, T. Sawada, Y. Kawaguchi, **2012**, 39 (1-4), 583-588.
[47] J.C. Umavathi and A.J. Chamkha, *Int. J. Energy & Tech*., **2013**, 5 (20), 1-10.
[48] A.J. Chamkha, B. Mallikarjuna, R.B. Vijaya, and D.R.V. Prasada Rao, *Int. J. Numerical Methods for Heat and Fluid Flow*, **2014**, 24, 1405-1436.
[49] X. Zhang, and H. Huang, *Int. Commun. Heat and Mass Transfer*, **2014**, 51, 31-38.
[50] C. Stelian, *Magnetohydrodynamics*, **2014**, 50 (1), 91-100.
[51] D. Srinivasacharya and K. Hima Bindu, In: ICCHMT Conference, Warangal NIT, *Procedia Engineering*, **2015**, 127, 1150–1157.
[52] N. Kishan and B.C. Shekar, *J. Applied Science and Engineering*, **2015**, 18 (2), 143-152.
[53] C.Y. Wang, *Transport in Porous Media*, **2016**, 112 (2), 409-428.
[54] C. Revnic, T. Grosan, I. Pop and D.B. Ingham, *Int. J. heat and mass transfer*, **2011**, 54, 1734-1742.